Coordination Chemistry Reviews 549 (2026) 217366

Contents lists available at ScienceDirect

Coordination Chemistry Reviews

journal homepage: www.elsevier.com/locate/ccr

2D materials in ultrasound-driven cancer therapies: Correlating material characteristics with therapeutic performance

Nam Anh Tran [a], Hang Thu Ta [a,b,*]

[a] School of Environment and Science, Griffith University, Nathan, Queensland 4111, Australia
[b] Queensland Quantum and Advanced Technologies Research Institute, Griffith University, Nathan, Queensland 4111, Australia

ARTICLE INFO

Keywords:
2D materials
Sonodynamic therapy
Sonothermal therapy
Ultrasound
Cancer therapies
Synergistic therapies

ABSTRACT

Overcoming the limited penetration of phototherapies, ultrasound-based therapies (sonotherapies) have emerged as a promising cancer treatment due to their deep tissue reach and therapeutic efficacy. However, conventional organic sonosensitizers suffer from rapid clearance and poor solubility, limiting their effectiveness. In contrast, nanoscale sono-activatable agents, especially 2D materials, offer unique physicochemical properties, enhanced stability, and superior antitumor performance.

Beyond acting as nanocarriers or passive supports, 2D materials actively participate in sonotherapy and enable the combination of multiple treatment modalities, improving therapeutic synergy. This review first outlines the fundamental principles and conventional applications of sonotherapy. It then focuses on recent advances in 2D materials as sonosensitizers and sonothermal agents, categorizing them based on structural and functional characteristics.

We also discuss the mechanisms of ultrasound activation and how properties such as piezoelectricity, bandgap, and thermal conductivity contribute to treatment outcomes. Strategies to enhance these features—such as atomic doping, defect engineering, and heterojunction construction—are examined in depth. Finally, we highlight current progress, limitations, and challenges in translating 2D material-based sonotherapies into clinical practice.

This review offers a timely and comprehensive perspective on the emerging role of 2D materials in sonotherapy and the critical gaps that must be addressed to enable their clinical adoption.

1. Introduction

The advancement of nanotechnology, especially nanomaterials, provided us more promising alternatives to traditional cancer treatments that involved surgery, radiotherapy and chemotherapy. These conventional therapies are usually accompanied with poor biocompatibility, bleeding, poor-targeting delivery and adverse effects on surrounding tissues (*invasive*). The innovative applications of nanomaterials in cancer theragnostic usually not only suppress the tumors' growth but also eradicate them. However, there are still many limitations that hinder their clinical applications. Phototherapy, including photothermal [1–3] and photodynamic [4], are promising candidates for minimally invasive or noninvasive cancer treatments. Via controllable irradiation of external light and highly precise deliveries of nanomedicines, phototherapy offered more selective treatments at specific locations of tumors that prevented severe effects on normal tissues. However, the penetration ability of light is diminished by tissues that hinder the obliteration of deeply located neoplasms [5]. To iron out these limitations, alternative approaches relied on ultrasound could be used as effective weapons to fight cancer, especially resistant cancers. Unlike the light, ultrasound (US) irradiation provided deep penetration through skin and tissues which facilitated efficient deep-seated tumors' treatment [5,6]. There are two main ultrasound-based therapeutic modalities involving sonodynamic therapy (SDT) and sonothermal therapy (STT). SDT and STT relied on sonosensitizers which trigger production of reactive oxygen species (ROS) [7] or sonothermal agents that produce heat [8] under exposure to ultrasound, to gain therapeutic effects.

Application of ultrasound as alternative strategy overcomes the penetration limitation of light. The other critical barriers of phototherapy such as tumors microenvironment [9] and development of heat shock proteins [10] still require solutions. Moreover, monosonotherapies arduously gain the utter erasure of cancer despite the irrefragable tumoricidal effect [11]. The conventional sonosensitizer are mainly based on organic compounds, especially porphyrin derivatives.

* Corresponding author at: School of Environment and Science, Griffith University, Nathan Campus, Brisbane, QLD 4111, Australia.
E-mail address: h.ta@griffith.edu.au (H.T. Ta).

https://doi.org/10.1016/j.ccr.2025.217366
Received 15 September 2025; Accepted 6 November 2025
Available online 17 November 2025

These compounds are easily degraded and quickly eliminated from human body despite their good sonodynamic performance in ROS production. Their poor solubility in water is also a critical hindrance for future clinical translation [12]. Obviously, sono-activatable agents have pivotal roles in performance of sonotherapies [13]. Therefore, the novel sonosensitizers or sonothermal agents that not only improve sonodynamic or sonothermal performance but also allow the synergistic combination of therapeutic modalities to gain superior tumoricidal effects are urgently needed. The flourishing advancements of multifunctional nanomedicines in recent years opened novel avenues for synergistic treatment strategies based on sonotherapies that bridge the gap to attain complete tumors removal in animal studies [14–16].

Due to the largest surface with many functional groups compared to other dimensional nanomaterials, 2D materials are extremely attractive materials for various applications, especially biomedicine. Their unique physicochemical properties such as biocompatibility, easy metabolism and targeting delivery, etc. made them as a research hotspot in disease diagnosis, therapy and drug delivery [17]. In sonotherapies, 2D materials could act as nanocarrier, sono-activatable agents and supporters for sonotherapies as well as ultrasound-based synergistic modalities. As nanocarriers, large surface and functional groups allow modification of 2D carriers with active compounds like drugs, gas donors, organic sonosensitizers or targeting molecules. These modifications not only improve therapeutic efficacy via combinational strategies but also provide high-targeting delivery via tumor recognition abilities. As sono-activatable agents, 2D materials, especially 2D semiconductors, could have notable contribution to SDT and STT via piezoelectric effects and electron movements owing to their relative narrow bandgap and suitable positions of energy bands. Under ultrasound excitation, 2D semiconductors trigger ROS or heat production through migration of electron-hole pairs to form charged surfaces for redox reactions. However, the easy recombination of electron-hole pairs compromises the sono-activatable performance of 2D materials. Metal single atoms doping, heterojunction construction and defect introduction are main approaches that restrain the recombination and facilitate separations of electron-hole pairs via narrowing the bandgap and trapping electrons. As the supporter, some 2D materials can support SDT and STT via GSH depletion and decomposition of H_2O_2 to supply oxygen for SDT and ameliorate hypoxia conditions although they do not possess sono-activatable properties. In addition, some 2D sono-activatable also have photothermal, photodynamic, chemodynamic and gas release effects that enable the integration of sonotherapies and other strategies to significantly aggrandize tumoricidal effects, in particular utter tumor eradication instead of merely tumor growth suppression [18,19].

So far, many reviews have discussed nanosonosenstizer [20], sonothermal agents [21], and recent advances in sonodynamic therapy [22]; however, they focused virtually on SDT and STT mechanisms, combination of sonotherapies and other therapeutic strategies, advantages and drawbacks, and categorizing sonosensitizers based on organic and inorganic compounds regardless of material shapes. The lack of reviews focusing on the role of the physical characteristics of sonosensitizers and sonothermal agents in the outcomes of ultrasound-based cancer therapies represents a significant gap in the advancement of sonotherapy. Additionally, there has been no review on the use of 2D materials in sonotherapies. Hence, in this comprehensive review, we aim to focus mainly on the applications of 2D materials in ultrasound-based cancer therapeutic strategies, summarizing recent progress, analyzing in-depth the correlation of 2D materials' properties and their performance in sonotherapies, and finally discussing benefits and challenges of 2D sono-activatable agents. In addition, fundamental information including SDT and STT mechanisms, piezoelectric effects, sonoluminescence and basic information of ultrasound is also provided to have comprehensive view about the development of sonotherapies based on nanomaterials in recent years.

2. Conventional application of ultrasound in cancer treatment

2.1. Ultrasound

Ultrasound (US) is high frequency soundwaves (>15 kHz) and above human hearing range. The most popular application of ultrasound is clinical diagnosis. However, in recent years, using of US as a cancer therapeutic tool has been paid special attention. There are two main types of US including low-intensity ultrasound (LIUS) and high-intensity ultrasound (HIUS). LIUS is ultrasound irradiation in which the intensity is lower than 3 W/cm^2. This kind of US is applied widely in theragnostic because of minimal thermal effects on tissues and targeting stimulation. On the other hand, the HIUS is ultrasound that intensity is higher than 5 W/cm^2. Because of its thermal and mechanical effects on tissues, it is usually considered as invasive and non-targeting sonication. A typical type of HIUS used in biomedical applications is high-intensity focused ultrasound (HIFU) which offers highly targeting irradiation. Besides providing stimulation for SDT and STT, application of US could improve not only the transportation of medicines but also enhance drug permeabilities by inducing pore formation in cell membranes [23].

2.2. Sonodynamic therapy (SDT)

Sonodynamic therapy is a therapeutic modality in which special agents, called sonosensitizer, are activated under irradiation of US to produce reactive oxygen species (ROS) including singlet oxygen ($^1O_2$), hydroxyl radical (*OH) and superoxide anion ($^*O_2^-$). These active ROS damage cellular DNA and proteins that induces cell apoptosis [24].

Based on the type of ROS generated under US irradiation, SDT can be divided into 2 types, named Type I and Type II. Type I is related to the formation of ROS radicals (*OH, O_2^{*-}, etc.) from cell substrates. This SDT type is not dependent on intracellular oxygen concentrations and not influenced by tumors hypoxic conditions. On the other hand, Type II is relied on the formation of singlet oxygen ($^1O_2$) from molecular O_2. Therefore, this type usually consumes more oxygen and has limited effects under hypoxia [25–27].

Sonosensitizers are compounds whose structures allow the excitation to transfer energy from ground state to higher energy one via US energy absorption. When the transition from high energy level to lower energy one occurs, released energy will be adsorbed by molecules to produce cytotoxic radicals [7]. Conventional sonosensitizers are organic compounds attributed to porphyrin derivatives (photophrin, hematoporphyrin and tetratolyl porphyrin, etc.) and organic dyes (IR780, methylene blue, emodin and acridine orange, etc.). Despite excellent stability, these compounds have low bioavailability, poor solubility (porphyrins, IR780 and curcumin) and high clearance rate in human body [5].

2.3. Sonothermal therapy (STT)

The US exposure can elevate tissue temperature locally via energy absorption, leading to the formation and explosion of microbubbles (acoustic cavitation). Traditional STT usually utilized only US, especially HIFU, to trigger thermal effects. Although HIFU can immediately increase temperature of irradiated areas to more than 50 °C that resulted in hyperthermia or thermal ablations, there are still many limitations that must be addressed. HIFU focal point is small (1–3 × 3–8 mm) [28] that led to the inadequately heating in large tumors [29]. Moreover, high energy US wave is reflected by gas and bones that reduced the therapeutic efficacy on tumors in bowel or located under bones structures [30]. The high augmentation of temperature (>50 °C) could cause serious damage on normal tissues despite effective tumor ablations. On the other hand, the mild thermal elevation can alleviate adverse effects on normal cells but trigger the heat shock proteins' release to counteract treatment [10].

2.4. In vitro and in vivo models used to evaluate sono-therapeutic performance

As mentioned above, ROS and heat generation are two critical factors in US-driven cancer treatments. A material that can induce higher levels of ROS or heat under US stimulation is expected to exhibit enhanced therapeutic performance. However, it is challenging to substantiate the therapeutic efficacy of material without experimental evidence confirming the presence and quantification of ROS or heat, which are essential for explaining and comparing therapeutic performance between different nanomedicines, as well as for demonstrating the benefits obtained from material modifications. This section will therefore focus on ROS detection and heat measurement, as well as in vitro and in vivo models used in investigations of sonotherapies.

For ROS generation, there are 2 main types of ROS related to sonotherapies, which are singlet oxygen ($^1O_2$) and hydroxyl radicals (*OH). Singlet oxygen is usually detected by using UV–Vis such as 1,3 diphenylisobenzofuran (DPBF), 9,10-Anthracenediyl-bis(methylene)dimalonic acid (ABDA) or fluorescent probe such as singlet oxygen sensor green (SOSG). Both DPBF and ABDA react with singlet oxygen to form endoperoxides which lead to the decrease in UV–Vis absorption at range from 350 to 420 nm. DPBF can react with 50 % singlet oxygen created during US irradiation while ABDA can trap up only 2 %. However, ABDA is more specific to $^1O_2$ compared to DPBF [31]. On the other hand, SOSG detect $^1O_2$ via the increase of fluorescent emission at 525 nm under excitation of 500 nm. This fluorescent probe is more sensitive than both DPBF and ABDA, however, its cost is more expensive [4]. The presence of *OH radicals is usually proved by utilizing UV–Vis probes such as *o*-phenylenediamine (OPD), 3,3′,5,5′-tetramethylbenzidine (TMB), 2,2′-azino-bis(3-ethylbenzothiazoline-6-sulfonic acid) (ABTS), methylene blue (MB) as well as fluorescent probe terephthalic acid (THA). The production of *OH will lead to the augmentation of UV–Vis absorption of ABTS and OPD at wavelengths of 734 nm and 415 nm, respectively. On the other hand, the absorption of TMB and MB at ~652 nm will diminish under presence of *OH. THA are usually used to detect *OH via the formation of fluorescent compound-2-hydroxyterephthalic acid that emit at 420 nm under excitation wavelength of 315 nm [32,33]. Another method to detect ROS generation is Electron Paramagnetic Resonance (EPR) measurement. However, compared to UV–Vis absorption and fluorescent emission-based methods, EPR require more specific equipment and higher cost. 5,5-dimethyl-1-pyrroline N-oxide (DMPO) and 2,2,6,6-tetramethylpiperidinyl-1-oxide (TEMPO) are commonly used as trapping agents for *OH and $^1O_2$, respectively [34]. For heat production, infrared thermal cameras are usually used to investigate the real-time changes of temperature during sonothermal therapy [8].

In vitro experiments commonly employed to evaluate sonotherapeutic performance include cell viability assays, intracellular ROS detection, and in vitro sonotherapy studies. For ROS detection, 2′,7′-dichlorofluorescein diacetate (DCFH-DA) is typically used by incubating cells with the probe. In the presence of ROS, the fluorescence intensity of DCFH-DA markedly increases, indicating oxidative stress levels [4]. Cell viability assays are valuable not only for assessing intrinsic cytotoxicity (without ultrasound exposure) but also for determining the therapeutic efficacy of nanomedicines against cancer cells. Various staining methods are used for this purpose, including UV–Vis absorption assays such as CCK8 [4], methylthiazol tetrazolium (MTT) [35], etc., as well as fluorescence-based assays using Calcein-AM/propidium iodide (PI) staining [8], etc. Flow cytometry is also a powerful technique for quantitatively analyzing treatment outcomes of sonotherapies [36].

For in vivo evaluation, mice—particularly nude mice—are commonly employed to investigate the therapeutic effects of sonotherapies in animal models. Currently, two main tumor models are typically used: single-tumor [37] and bi-tumors (primary and distant tumors) ones [38]. The latter has gained popularity as it better mimics tumor metastasis. The treatment of primary tumors can lead to the suppressed proliferation of distant tumors via triggering of immune response by sonotherapies [39]. The tumor generation process usually follows the conventional procedure involving subcutaneous injection of cancer cells into the flanks of mice. Nanomedicines are typically administered via intravenous injections through the tail vein. To evaluate the tumoricidal effects of the nanomedicines, the tumor volumes are regularly recorded, and the tumor inhibition rate can be calculated using the following equations:

(1) Tumor volume:

$$\text{Tumor volume} = \frac{\text{Width}^2 \text{ x Length}}{2}$$

(2) Tumor growth inhibition rate (TGI)

$$\text{TGI}(\%) = \left(1 - \frac{V_r^x}{V_r^c}\right) * 100\%$$

in which V_r^x is the relative tumor volume of treated groups (x), V_r^c is the relative tumor volume of control group (c). Relative tumor volume is determined by dividing tumor volume measured on day n by the tumor volume measured on day begin the treatment [40–43].

2.5. Tumor environment (TME) and its effect on sonotherapeutic performance

Due to the metabolic abnormalities and uncontrolled proliferation, the tumors usually need more oxygen to produce energy to afford the requirement for growth [44]. Moreover, the rapid division usually leads to the highly dense accumulation of cancer cells in solid tumors. These results in the imbalance between oxygen supply and requirement, finally induce the formation of hypoxic and necrotic tumor areas that are 100 μm far away from blood vasculature [45]. Hypoxia, the state of low oxygen levels in tumors, can lead to the production of hypoxia-inducible factors (HIF) and activation of heat-shock proteins that improve the resistance of cancer cells toward therapies via promoting their survival and migration [46,47]. The hypoxia condition usually promotes NOX4 expression which main oxidation product is H_2O_2. Therefore, the level of H_2O_2 in cancer cells is typically higher than normal ones. The increase of H_2O_2 level is crucial key for up-regulation of antioxidants like glutathione that induce detoxification and clearance of ROS. Moreover, the accumulation of H_2O_2 also activates the transcription factors and impedes suppressor genes to support uncontrolled proliferation [48,49]. In addition, TME also triggers immunosuppression that prevents the natural tumoricidal effects of immune cells [50].

The sonotherapies, including SDT and STT, are based on generation of ROS and heat to induce apoptosis on cancer cells. Under hypoxia conditions, low level of oxygen typically leads to insufficient conversion into singlet oxygen. Together with promotion in survival caused by HIF, the therapeutic performance of SDT can be inhibited significantly. Moreover, the production of heat shock proteins under hypoxic are the main obstacles for STT because these proteins improve the heat resistance of tumors. GSH also contributes to diminishing therapeutic outcomes of both SDT and STT via scavenging ROS by triggering antioxidant defense system [9].

Therefore, reversing TME can provide more benefits for sonotherapies. There are many strategies that were used to attenuate the TME include:

(1) Decreasing H_2O_2 level via its decomposition into O_2 or hydroxyl radicals. The decomposition of H_2O_2 into O_2 is powerful tool that not only relieves the hypoxia condition to suppress the expression of HIF but also supplies more oxygen source for conversion into

singlet oxygen. These positively contribute to enhancement of treatment outcomes of SDT. The conversion of H_2O_2 into *OH radicals, on the other hand, provides chemodynamic effects that increase ROS level to improve the death of cancer cells. Moreover, the presence of H_2O_2, in some cases, can provide gas therapy via the release of NO gas [9,51,52].

(2) Depleting GSH level via consuming GSH or suppressing metabolic pathways that produce GSH. Inhibitors such as Glutamate-cysteine ligase (GCL) and buthionine sulfoximine (BSO) can suppress GSH synthesis [53]. Moreover, some metal compounds can reduce GSH into glutathione disulfide (GSSG), resulting in GSH depletion [54–56].

3. 2D materials mediated ultrasound-based cancer therapy

3.1. 2D materials in bio-applications

2D materials have thickness from single to few atoms' layers. Due to their ultrathin structure, 2D nanomaterials have extremely large surface (high surface/volume ratio) and exposed atoms that facilitated to not only the functionalities but also transmission of energy and fast response time [63]. Moreover, large surface with π-π stacking interactions permitted the easier surface modification with bioactive compounds, polymers, antibodies and receptors that not only improved chemical/physical properties such as hydrophobic, hydrophilic, stability or biocompatibility but also allowed the high targeting delivery as effective nanocarriers [64]. The ultra-thinness of 2D nanomaterials also helped them prolong the circulation time and enhance cellular permeability. Due to specific properties, 2D materials can be applied as biosensor [65], drug delivery, bioimaging, therapies agents [66]. As therapies agents, 2D nanomaterials played vital roles in many therapeutic modalities for various diseases, especially cancer. In cancer therapy, various 2D nanomaterials including black phosphorus, carbon nitride and its derivatives, layered double hydroxides, transition metal dichalcogenides and oxides, MXenes, metal organic frameworks (MOFs), covalent organic frameworks (COFs), polymers, silicene, graphene and its derivatives and boron have been utilized for various therapeutic strategies [67,68], particularly sonotherapies.

3.2. 2D materials as nanocarriers

As mentioned above, organic sonosensitizers, especially porphyrin derivatives, are hydrophobic and poor bioavailability that diminish the circulation time and rapid degradation from human organism despite stable performance and high selectivity to tumors. These barriers debilitate SDT therapeutic effects [69,70]. Nanocarriers seem to be promising solutions to overcome these limitations and improve permeability and retention effects that enhanced therapeutic effectiveness. 2D materials are promising candidate for high targeting delivery to specific tumor areas because they are ultrathin and have extremely large surface (high surface to volume ratio). Moreover, functional groups on surface and edge facilitate covalent binding of bioactive compounds [71]. Oxidized-graphitic carbon nitride (OCN) nanosheet modified with Chlorin e6 (porphyrin sonosensitizer) and NO donor *N*,*N*-di-sec-butyl-N, N-dinitroso-1,4-phenylenediamine (BNN6) has been developed for synergistic gas/sonodynamic therapy on 4 T1 cells. Graphitic carbon nitric merely played a role of a nanocarrier with functional carboxyl groups that facilitated conjugation with sonosensitizer Chlorin e6 via PEG-NH2 modification. The NO donor was bonded on surface of carbon nitride via π-π stacking and hydrophobic interactions. OCN did not have SDT effect under US irradiation [72]. Reduced graphene oxide (rGO) nanosheets/mesoporous silica nanocomposite modified with iron-oxide has been used as nanocarrier for sonosensitizer Rose Bengal. This magnetically navigational delivery not only enhanced specific accumulation of sonosensitizer at tumor site but also improved the SDT effects via promoting ROS production as well as cavitation [73].

3.3. 2D materials mediated sonodynamic therapy (SDT)

3.3.1. Piezoelectric effect, sonoluminescence and ROS generation

Under US irradiation, sonosensitizers trigger the generation of ROS to induce cancer cell apoptosis via 2 main mechanisms including sonoluminescence and piezoelectric effects. While sonoluminescence is mainly related to conventional organic sonosensitizers, piezoelectric effect is the main reason for ROS production from almost novel inorganic, organic and combinational inorganic/organic ones. To provide a clearer understanding of SDT, this review thoroughly summarizes its underlying mechanisms along with the fundamental principles involved in the design of sonosensitizers.

3.3.1.1. Sonoluminescence. Under ultrasound stimulation, cavitation bubbles are formed and collapse incessantly. The explosion of microbubbles results in the blackbody radiation, bremsstrahlung radiation and recombination radiation or combination of these radiations. These trigger the emission of light, sonoluminescent light, that interacts with sonosensitizers to excite them moving from ground state (So) to transient excited single state (Sn). This allows ROS generation via interaction between sonosensitizers and cell substrates [12,20]. Sonoluminescence is the main mechanism behind the sonodynamic performance of conventional organic sonosensitizers and metal organic framework (MOF)-based sonosensitizers, which are constructed from sono-activatable organic ligands. In contrast, the 2D materials discussed in this review exhibit sonodynamic effects primarily through their piezoelectric properties. Therefore, our focus is mainly on the piezoelectric mechanism.

3.3.1.2. Piezoelectric effect

3.3.1.2.1. Piezoelectric mechanism and Piezoelectric ROS generation. Piezoelectric effect is the physical phenomenon, in which negative and positive charge in the centers of materials launched the displacement to surface in response to external mechanical strain/stress. The interaction between dielectric and elastic characteristics of materials via intrinsic coupling is key reason for this effect. While dielectric properties involve the electron movement under electric field, the elastic properties relate to stress and strain [74]. Under mechanical stresses including tension and compression, the crystal structure of materials is deformed via reconfiguration and rearrangement of dipoles that are caused by ions' shifts in unit cell in a particular direction [75,76]. This results in the electric dipole moment that facilitates generation of piezoelectric potential to trigger the polarization, in which electric charges move to the opposite ends of materials, accumulate there and to form energy bands. US is one kind of mechanical forces [77]. Under tensile and compressive stresses induced by ultrasound irradiation, the electrons are excited and embarked on the transportation from valance band (VB) to conduction band (CB). This triggers the separation of electrons (−) and holes (+) pairs and their accumulation at ends of materials to cause the oppositely charged surfaces. Electric charges at these surfaces, usually called surface-free charges, will interact with intracellular molecules to trigger ROS generation. These processes usually involve continual release and absorption charges at energy bands. If the CB potential was more negative than −0.33 V ($E_{O2/O2\cdot-}$), singlet oxygen can be produced. If the VB potential was more positive than 2.01 V ($E_{H2O/*OH}$), *OH can be formed. Another mechanism to describe US-induced ROS production is energy-band bending theory. Under US irradiation, piezoelectric polarization induces the bending of band energies via internally polarized electric field [78] that result in the change of values at the edges of both CB and VB, usually more positive VB and more negative CB. Electric charges at these changed edges will react with intracellular molecules to produce ROS. This explains why some semiconductors still perform catalytic properties in ROS generation although their original energy bands are not suitable for singlet oxygen or hydroxyl radicals' production [79]. The lattice, organization of atoms and molecules in materials

structure, has crucial effects on their piezoelectric properties. The lattice modifications that alter lattice symmetry can promote displacement of charge centers in one direction of lattice (polarization degree). Improvement of polarization degree results in amplification of materials piezoelectric properties that directedly influence sonodynamic therapeutic efficacy. Materials that are more non-centrosymmetric have the better piezoelectric performance due to the easier movement of atoms or charge centers under mechanical excitation [22].

2D materials, such as carbon nitride, phosphorus and layered double hydroxides, etc. were non-centrosymmetric semiconductors; therefore, they could perform as sonosensitizers under US irradiation via piezoelectric effect. The crucial barriers that prevented these piezoelectric sonosensitizers gaining effective sonodynamic performances are the rapid recombination of electron-hole pair, unsuitable positions of CB or VB, and relatively wide bandgap that hinder charges separation. To surmount these limitations, doping with metals, forming deficient structures and heterojunction are useful strategies.

3.3.1.2.2. Doping with metals. Metal doping involves introducing metal ions or single atoms into sensitizer structures to enhance their performance. The anchoring of metal ions or atoms in structures introduces lattice distortion that regulates non-centrosymmetric property of materials and alters local polarization that facilitate easier displacement of charges. In addition, the alterations between some intrinsic atoms with extrinsic atoms result in significant changes in electronic properties due to the difference in valance. The extra charges (electron/hole) formed via the elements exchange migrate to energy bands and have weak bindings with surrounding atomic lattice. Due to the weak bindings, energy levels of these charges are usually below CB or above VB of the un-doped materials. These lead to the introduction of new bandgaps that is narrower than the original bandgaps of un-doped materials to promote electron-hole pairs separation. Moreover, metal dopants also generate charge traps that hinder the recombination of electron-hole pairs. As a result, piezoelectric performance of doped-sonosensitizers is significantly improved under ultrasound stimulation [80–82]. In addition to improvement in sonodynamic effects, metal-doping offers additional therapeutic benefits, including chemodynamic therapy, glutathione (GSH) depletion, and cuproptosis (particularly with copper doping). However, the doping concentration is critical. While an optimal doping level can markedly enhance performance, excessive doping may create recombination sites instead of electron traps, thereby reducing ROS generation via compromising piezoelectric performance [83].

3.3.1.2.3. Deficient structures. Virtually, deficient structures were constructed by introducing vacancies or defects into crystal lattice via specific processes including annealing [32], etching [83], in situ redox [84], etc. The introduction of vacancies or defects could cause significant changes in lattice and make materials become more non-centrosymmetric. This amplifies piezoelectric performance via altering local polarization environments. Moreover, the formation of vacancies creates unpaired electrons and unsaturated centers that contribute to alteration in electronic structure of materials and further lead to adjustment of bandgap. The presence of vacancies also influences recombination of electron-hole pairs via creation of additional energy states [85] and electron traps that capture charges to depress this phenomenon. However, not all types of vacancies have a positive role in improving piezoelectric performance [86]. Like metal-doping, the excessive introduction of defects like vacancies can compromise sonodynamic efficacy due to the formation of recombination sites instead of electron traps.

3.3.1.2.4. Heterojunction structures. The combination of two semiconductors creates an interface area at their contact, known as a heterojunction. [87]. The formation of heterojunction structures could enhance electron-hole separation via modifying bandgap or altering positions of CB or VB band. Moreover, the redistribution of surface charges at heterojunction also contributes significantly to prevention of charges recombination. Therefore, these effectively boost sonodynamic performance of sonopiezoelectric-sensitizer.

There are many types of heterojunctions including type I, type II and type III, *Z*-scheme and S-scheme. In type I, electrons and holes of semiconductor A will migrate to semiconductor B (electrons go to CB and holes go to VB). Concomitantly, electrons and holes in semiconductors B are also separated under US. The migration of electrons and holes from semiconductor A can increase the accumulation of charges in semiconductor B that results in easier recombination. That is not beneficial for piezoelectric effects. In type II, electrons at CB of semiconductor A will move to CB of semiconductor B, while the holes at VB of semiconductor B will move to VB of semiconductor A. This leads to the improvement in electron-hole pair separation that enhances piezoelectric effects. In type III, the energy gaps of semiconductor A and B are intensely different; thus, the bandgaps of semiconductor do not overlap that does not allow any charges movements between them [88]. In S-scheme and *Z*-scheme, if CB of semiconductor A (oxidative) and VB of semiconductor B (reductive) are close enough, electron at CB of A will migrate to VB of B and recombine with hole of B. This eliminates the recombination of electrons at CB of B and holes at VB of A. Therefore, the redox potential of electrons at CB of B and holes at VB of A are retained. This is favorable for piezoelectric ROS generations and sonodynamic performance of sonosensitizers. This strategy is useful for combination between 2 semiconductors which energy bands are only suitable for singlet oxygen or *OH generation. For example, if semiconductor A have suitable VB for *OH production but its CB is not favorable for $^1O_2$ generation while semiconductor B have reverse energy bands that is favorable for $^1O_2$ generation but unfavorable for *OH production, the combination of these semiconductors (if they have satisfactory energy bands) could create heterojunction that is appropriate for both $^1O_2$ and *OH generation [89]. The difference between *Z*-scheme and S-scheme is simultaneity of excitation and redox mediator. The Z-scheme has sequential excitation. In Z-scheme, one semiconductor will be excited first, and the electron-hole pairs separation is triggered. These electrons will be transferred to redox mediator. Oxidized form of redox mediator will lead to the excitation of second semiconductor that separates their electron-hole pairs. On the other hand, the S-scheme has simultaneous excitation that excites 2 semiconductors at the same time and causes the charge migration immediately. Accordingly, *Z*-scheme, S-scheme and type II heterojunction are beneficial for piezoelectric effects; thus, these heterojunction types are widely used in constructing novel sonosensitizers based on combination of 2 semiconductor to promote sonodynamic performance in SDT.

3.3.2. 2D sonosensitizers – Multifunctional candidates for synergistic modalities

Many approaches, which utilize different kinds of 2D sonosensitizer in SDT, have been investigated in recent years. Virtually, these approaches relied on piezoelectric effect to trigger ROS generation under US. However, some 2D nanosheets gained sonosensitive properties via combination with organic sonosensitizer in their structures. In this review, 2D nanosensitizers are classified into nine main groups.

Not only provide promising sono-activatable therapeutic effects, many 2D nanosensitizers could play important roles in reversing TME and allowing combination between SDT and other treatment modalities, for example phototherapies, chemodynamic, chemotherapy, gas therapy, immunotherapies and starvation therapies. These abilities of 2D sonosensitizers can either be intrinsically possessed or achieved through structural modifications.

Many 2D sonosensitizers, especially ones containing metal compounds or ions. Typically possess abilities to actively reverse TME via attenuating H_2O_2, supplying O_2 and depleting GSH.

(1) Converting H_2O_2 into hydroxyl radical (*OH) and GSH consuming: this ability is typically achieved by metal-based sonosensitizers containing compounds or ions of iron [90], copper [91], etc. These metal species can catalyze *OH production

through Fenton or Fenton-like reactions. Moreover, the presence of these metal species can also convert GSH into GSSG [92,93], thereby actively depleting intracellular GSH levels. Collectively, these contribute to modulating the TME and enhance the SDT performance. However, some 2D sonosensitizers belonging to the carbon nitride family, such as polyheptazine imide, possess intrinsic Fenton-like catalytic activity even though they do not contain any metal ions [33,94].

(2) Supplying oxygen sources to mitigate hypoxia and enhance the conversion into $^1O_2$: this ability is usually achieved by 2D sonosensitizers containing Manganese based compounds [95] and noble metals including Pt [96], Pd [97], etc. These metal species can catalyze the decomposition of H_2O_2 into O_2 that not only relieve hypoxic conditions to prevent the expression of HIF but also provide an oxygen source for SDT. These promote the SDT therapeutic outcomes significantly.

Synergistic modalities based on SDT,

(1) *SDT and other ROS-based therapies (photodynamic (PDT)and chemodynamic (CDT))*: some 2D sonosensitizers can facilitate these combinations via either their intrinsic property or structural modification. MOFs or COFs that are constructed from porphyrin-based ligands can perform both SDT and PDT because porphyrin compounds can be excited by both US and light irradiation. MXenes and LDHs can possess catalytic activity for Fenton reaction via metal ions in their structure or modifications including doping and heterojunctions. Polyheptazine imide (carbon nitride) has intrinsic catalytic properties for CDT. The other sonosensitizers usually gain their Fenton catalytic activity or PDT properties via modifications including doping, heterojunctions or binding on surface with sono-activatable ligands. These combinatory modalities usually enhance therapeutic performance of SDT via the amplification of ROS levels via production of both $^1O_2$ and *OH. More ROS generation boost oxidative cell death [98]

(2) *SDT and heat-based therapies (photothermal therapy-PTT)*: this synergistic modality is typically facilitated by MXenes, black phosphorus (BP), TiO_2 and Sn nanosheets, etc. due to their high photothermal conversion efficiency as well as the heterojunction structures between 2D sonosensitizer and photothermal agents such as Au nanorods and rGO, etc. The concurrent production of heat and ROS can improve treatment outcomes via overcoming limitations each modality alone [99], for example, the adaptation of cancer cells to monotherapy. While ROS generation promotes sensitivity of tumors with heat, heat production can improve oxygen supply for SDT via the increase of blood flow to tumors [100].

(3) *SDT and immunotherapies*: 2D sonosensitizers possess large surface area with many functional groups. This facilitates binding with immunoadjuvants [101] [102] that allows the combination between SDT and immunotherapies. In addition, SDT can also trigger immune response via immunogenic cell death (ICD) pathway [97,103]. ROS generation triggers the release of ICD mediators including pathogen-associated molecular patterns (PAMPs) and danger-associated molecular patterns (DAMPs) via apoptosis of cancer cells. These mediators enhance the maturation of dendritic cells and stimulation T cells to kill tumors. Some 2D sonosensitizer containing Mn^{2+} [104] and Pt [105] can cause the DNA damage to trigger cGAS-STING pathways. These combinations not only perform therapeutic effects on primary tumors but also provide immune response to suppress the metastasis and growth of distant tumors [106].

(4) *SDT and other therapies including chemotherapy, gas therapy, etc*: due to the large surface with many functional groups, 2D sonosensitizers are ideal carriers for delivery of chemodrug [107], and gas donors [108]. This supports the combination between SDT and other therapies that not only improve the therapeutic efficacy but also prevent the adaptation of cancer cells to monotherapy.

3.3.2.1. Graphene and its derivatives. Having hexagonal honeycomb lattice, most graphene and its derivatives are centrosymmetric materials, preventing piezoelectric performance of these 2D materials. They usually played roles of nanocarriers or supporters to SDT. However, some graphene quantum dots performed as promising sonosensitizers owing to their non-centrosymmetric structures. Water soluble graphene quantum dots (WSGQDs) was synthesized with specific functional group modified on surface. These groups not only prevented intermolecular π-stacking but also improve noticeably the water solubility of GQDs. Moreover, beside the deep-red photoemission that provided helpful tool for tracking, these GQDs also had the superior sonosensitivity. After 12 days of SDT treatment, these GQDs suppressed conspicuously the growth of Hep-G2 tumors [109]. Multifunctional N-doped carbon dots (CDs) with sulfur trioxide groups on the edge were synthesized from polyethylenimine and indocyanine green in assistance of microwave [110]. These dots have p-n junction conductivity and a greatly narrow bandgap (1.62 eV), facilitating charge separation under ultrasound irradiation. Additionally, holes formed during excitation could react with overexpressed GSH to ameliorate TME and further minimize negative effects of TME on SDT outcomes. These CDs performed excellent sonodynamic therapeutic efficacy via complete eradication of 143B tumors with only single time of injection and irradiation [110].

3.3.2.2. Carbon nitride (CN) and its derivatives. Based on tri-*s*-triazine (C_6N_7) units, a six-membered benzene ring in which three carbons are replaced with nitrogen, as elementary building blocks [111], carbon nitride (C_3N_4) and its derivatives possess an intrinsically non-centrosymmetric structure due to the lack of inversion center in these units. This allows them to exhibit piezoelectric response under US irradiation. Due to the stability, low toxicity and controllable bandgap (Eg = 2.7 eV) in which the CB band is usually more negative than −0.33 eV, C_3N_4 and its derivatives are promising sonosensitizers for SDT. However, the pure carbon nitride nanosheets usually exhibited weak piezoelectric performance owing to their fast recombination of electron-hole pairs at structural defects [94]. To overcome these barriers, doping with single atoms or repairing defects of structures are helpful solutions. C_3N_4 has been annealed with molten salts mixture (LiCl/NaCl) to repair defects and attain polyheptazine imide (PHI) structure. The repaired nanosheets have significantly improved ROS production when compared to unrepaired ones. After 14 days of SDT treatment using PHI as sonosensitizer, 4 T1 tumors have been suppressed notably [94]. The doping of C_3N_4 nanostructure with single atoms, especially metal atoms, could be useful in not only delaying the recombination of electron-hole pairs but also introducing narrower bandgap that facilitated the utilization of lower energy US to obviate potential damages to surrounding tissues. Iron doped C_3N_4 has provided 0.43 eV reduction of bandgap and enhancement in singlet oxygen generation via the more negative CB band when comparing to undoped carbon nitride. Not only supporting the SDT as a sonosensitizer, iron single atoms also allowed the synergistic combination with chemodynamic therapy for melanoma. Outstanding sonodynamic performance (tumor inhibition rate ~ 98 %) was obviously observed in B16F10 tumor-bearing mice treated with Fe doped C_3N_4 under ultrasound irradiation for 15 days. SDT treated mice had lifespan extended to 40 days [90]. Instead of anchoring Fe atoms on C_3N_4 nanosheets only, the simultaneous modification of their structure with nitrogen vacancies excellently improved ROS generation in the better way. Nitrogen vacancies could be electron traps that promoted electron accumulation at iron atoms. Therefore, the combinational modification (doping + nitrogen vacancies) boosted SDT/CDT therapeutic effect on 4 T1 cancer cells. Tumor inhibition index attained 81.45

% in mice treated with Iron doped Nitrogen vacancies C_3N_4 and ultrasound illumination after 14 days. This was striking evidence for tumor elimination ability of these sheets via SDT/CDT [32]. Another approach to improve sonopiezoelectric performance of C_3N_4 was combination with the other sonosensitizers. Large surface of protonated g-C3N4 (pCN) nanosheets were modified with Chlorin e6 (Ce6, organic sonosensitizer) to enhance sonodynamic effects under ultrasound as well as allow the combination with photodynamic/photothermal therapy. The binding of Ce6 did not cause any changes in the structure of these sheets and were a metal-free modification. Under concurrent irradiation of both 808 nm laser and US, the photo-sono-triggered ROS production was established to kill cancer cells. Moreover, pCN also owned photothermal and immune adjuvant effects in boosting the maturation of dendritic cells to activate immune response. After 21 days of treatment, 4 T1 tumors treated with photo-sonodynamic therapy became smaller and disappeared [112]. Fig. 1 shows recent efforts in SDT application of carbon nitrides.

3.3.2.3. Phosphorus. Due to high directional properties and non-centrosymmetric structure (orthorhombic honeycomb structure) [113], black phosphorus (BP) could be used as sonosensitizer via piezoelectric effects. A relatively narrow bandgap (approximately 0.84 eV) in which the CB band position is approximately −0.39 eV of BP accelerates the ROS production under US stimulation. In addition, BP nanosheets possess high photothermal conversion efficiency that facilitates the combination of SDT and PTT to attain synergistic therapeutic efficacy in tumor ablations. BP nanosheets have been applied for SDT treatment on 4 T1 tumor-bearing BALB/c mice. After 2 weeks, mice treated with BP and US showed significant suppression of tumor growth and metastasis without noticeable off-target toxicity on the other organs [114]. To improve the biocompatibility and targeting delivery of BP nanosheets, polyethylene glycol (PEG) and polyethyleneimine (PEI) [115], NH_2-PEG-RGD [116] and (1,2-distearoylsn-glycero-) [117] based phospholipids have been used.

BP is a monoelemental material, thus its piezoelectric properties are not quite excellent owing to the lack of ionic polarization [113]. To promote its piezoelectric performance that leads to enhancement of therapeutic outcomes, BP is usually combined with the other materials via doping or constructing multifunctional nanoplatforms that boosted ROS generation as well as facilitated concurrent multitherapy. Pt-modified black phosphorus nanosheets loading with L-arginine has been utilized for synergistic gas-sonodynamic therapy. Platinum contributed to decomposition of H_2O_2 into O_2 that not only relieved intracellular hypoxia but also supplied oxygen source for SDT. Moreover, the modification of Pt on BP surface also hindered the recombination of electron-hole pairs that allowed more effective ROS generation when compared to pure BP. L-arginine supplied NO that trigger cell apoptosis via interaction with H_2O_2. After 14 days, these nanoplatforms reduced the tumors size outstandingly in 4 T1 tumor-bearing mice [96].

Au nanoparticles anchored on BP have been modified with MnO_2 nanosheets to construct sono-activated nanoplatforms. The anchoring of gold nanoparticles on BP surface could trap electron via surface plasmonic resonance to inhibit the recombination of electron-hole pairs. The binding of MnO_2 nanosheets not only alleviated the hypoxia and amplified the SDT via O_2 supplementation from H_2O_2 but also enhanced MR imaging. MCF-7 tumors treated with these nanoplatforms were suppressed efficiently with US irradiation [118].

The combination of BP and TiO_2 provided photo-sonoactivated nanoplatforms. Both TiO_2 and BP were sonosensitized materials, so their amalgamation could improve SDT conspicuously. Not only be a sonosensitizer, BP nanosheets also offer excellent photothermal conversion. Under synchronous irradiation of US and light, these nanoplatforms provided synergistic photothermal-sonodynamic therapy for eradication of 90 % 4 T1 cells [115].

$FeSe_2$ anchored on BP ($BFeSe_2$) was utilized for bladder cancer SDT treatment. The modification with $FeSe_2$ reduced the bandgap from 1.30 eV to 0.97 eV, ameliorating electron–hole pair separation, thus aggrandized the ROS production under US excitation. MB49 orthotopic bladder tumors treated with $BFeSe_2$ were suppressed relatively under US irradiation [119].

BP nanosheets modified with IR780 (BPNSs@PEG-SS-IR780/RGD) served as multifunctional sensitizer for not only SDT but also photothermal and photodynamic therapies as well. Raji cell proliferation was inhibited completely via photo-sono multitherapeutic modality. BP nanosheets were utilized not only as photo-sonosensitizer but also as nanocarrier for IR780 [116]. Fig. 2 shows representative recent efforts in using black phosphorus nanosheets as nano-sonosensitizers.

3.3.2.4. Layered double hydroxides (LDHs). LDHs constructed from two metal ions including divalent and trivalent, have general formula $[M^{2+}_{1-x}M^{3+}_{x}(OH)_2]^{x+}(A^{n-})_{x/n}{\cdot}yH2O$ in which, A^{n-} are anions (nitrates, sulfates, carbonates) and y is number of water molecules filled interlayer gap between metal hydroxide layers and x is ratio of trivalent/(divalent + trivalent) metal ions. LDHs has lamellar structure. Due to the replacement of some M^{2+} cations by M^{3+}ones, LDHs usually have positive charged surfaces that are balanced by water molecules and anions in interlayer spaces [120]. In the bulk structure, LDHs do not show any piezoelectric response. When being dispatched into layers under external force, they became non-centrosymmetric structures due to the lack of their inversion symmetry and performed as piezoelectric materials [121]. This is the reason for their sonodynamic performance. Moreover, the presence of metal cations on the surface not only played as ROS productions catalysts but also supported the alleviation of tumor microenvironment (TME) via GSH depletion, H_2O_2 decomposition and hypoxia relief. To amplify the sonodynamic effects of LDHs, the metal-doping via ion exchanges between the other metals and two existing metals has been applied. Furthermore, LDHs are also effective nanocarriers for chemodrugs due to their pH-responsive property, large surface, biocompatibility and especially positive charged surface that were favorable to effectively bindings with negative cell membranes [122–124]. Table 1 demonstrated recent strategies utilized 2D layered double hydroxides as nanosonosensitizers for SDT.

Table 1 provides compelling evidence of the antitumour effects of 2D LDHs under ultrasound activation, with tumor growth inhibition rates generally exceeding 70 %. Enhanced tumor suppression was observed in materials that enabled the combination of SDT with other therapies, including immunotherapy, chemodynamic therapy (CDT), and starvation therapy. However, due to variations in treatment dosages, ultrasound parameters (intensity, duration, and frequency), and underlying tumor-targeting mechanisms, it remains challenging to directly compare the sonodynamic therapeutic performance across different 2D LDHs. Fig. 3 represents recent studies on 2D LDHs mediated SDT.

3.3.2.5. MXenes. MXenes, a novel class of 2D materials, have formula of $M_{n+1}X_nT_x$ in which M is transition metals, X is carbon and/or nitrogen, and T stands for surface termination groups such as fluorine, oxygen, chlorine, and hydroxyl. MXenes have special properties including large surface, superior electrical conductivity, biocompatibility and non-toxic in vivo [132]. Moreover, MXenes could perform as both metal and semiconductor [133]. Under US irradiation, the deformation of the non-centrosymmetric lattice occurs and triggers piezoelectric polarization that allows ROS generation if CB band is more negative than −0.33 eV [134]. However, solitary MXenes are rarely used as sonosensitizer. They are typically modified to construct heterojunctions that not only narrow the bandgap but also restrain the recombination of electron-hole pairs. Main strategies for fabricating these heterojunctions include converting metal ions in MXenes into metal oxides through the introduction of oxygen defects or in situ oxidation [135], as well as incorporating other sonosensitizers [136] or noble metals [137]. These modifications not only contributed significantly to enhancement of MXenes sonodynamic

A. 2D MATERIALS IN SONOTHERAPIES AND THEIR MECHANISMS

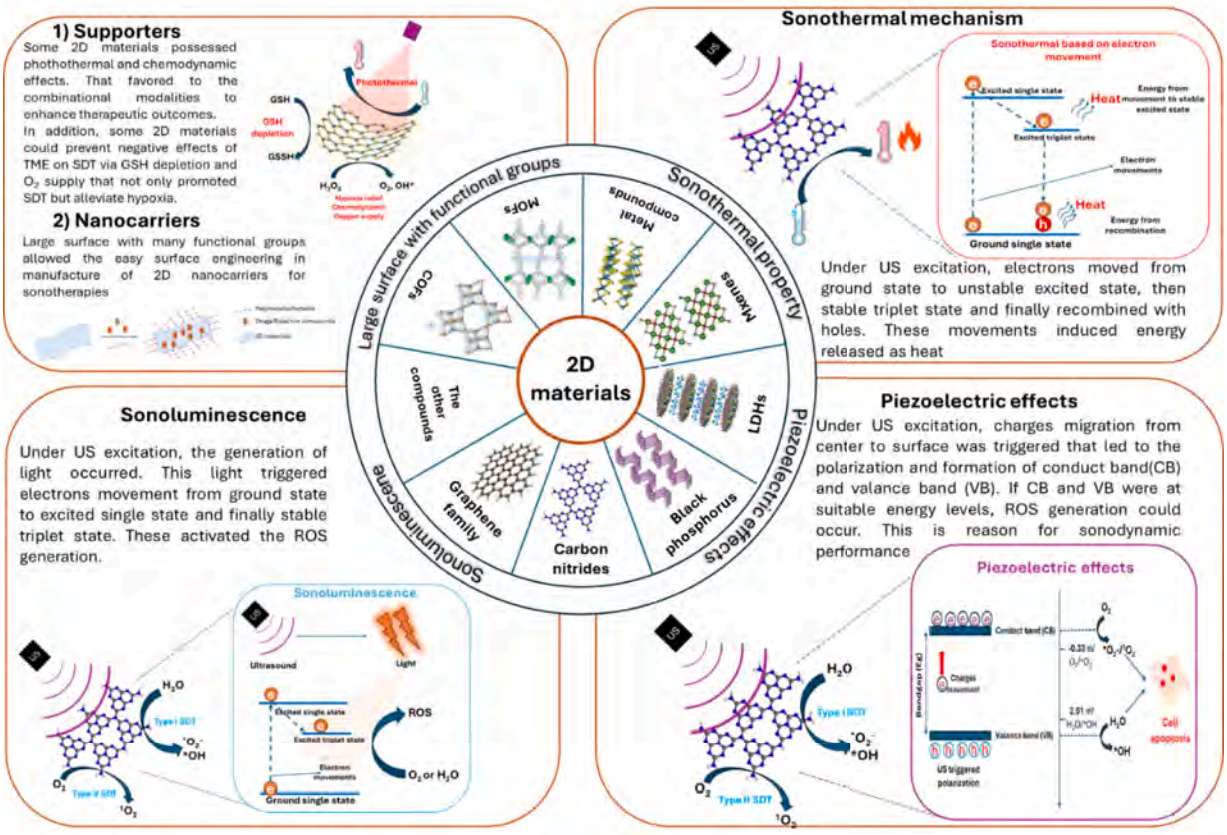

B. STATEGIES FOR IMPROVEMENT OF SONOTHERAPIES OUTCOMES

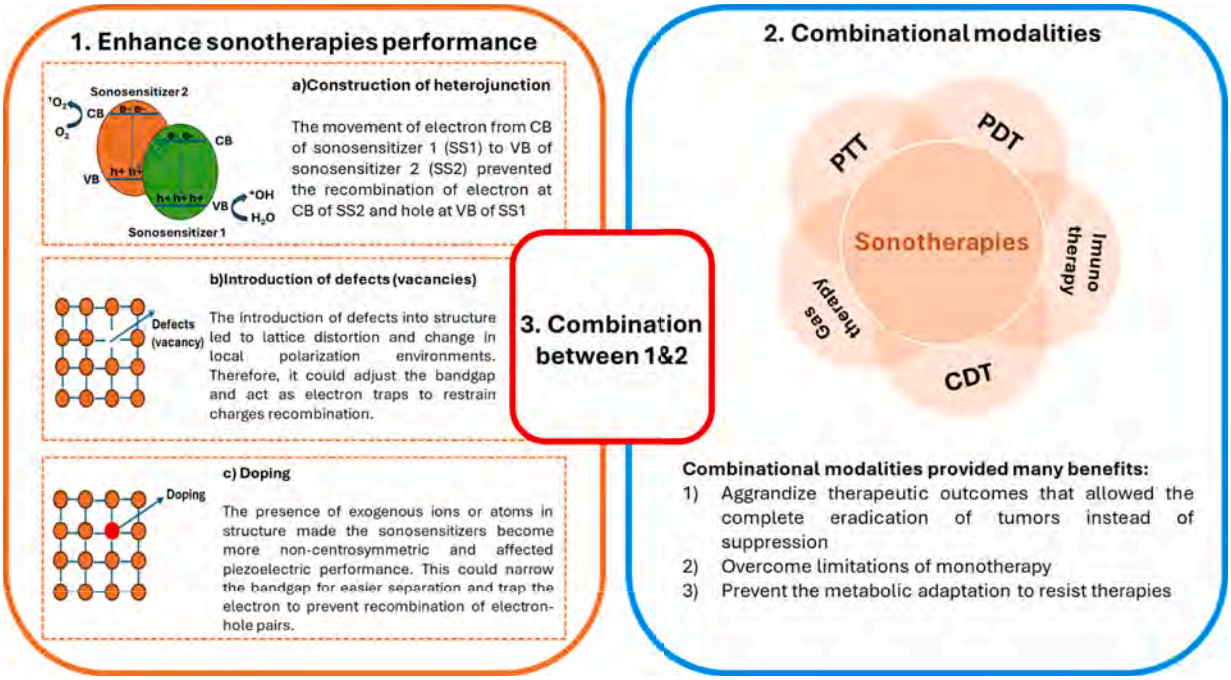

Scheme 1. Schematic illustration of applications of 2D materials in ultrasound-based cancer therapies. A. Roles of 2D materials in sonotherapies and these mechanisms, **B.** Strategies used to improve therapeutic efficacy of sonotherapies. The structures of 2D materials used in Scheme 1.A is reproduced with permission from papers. [57–62]

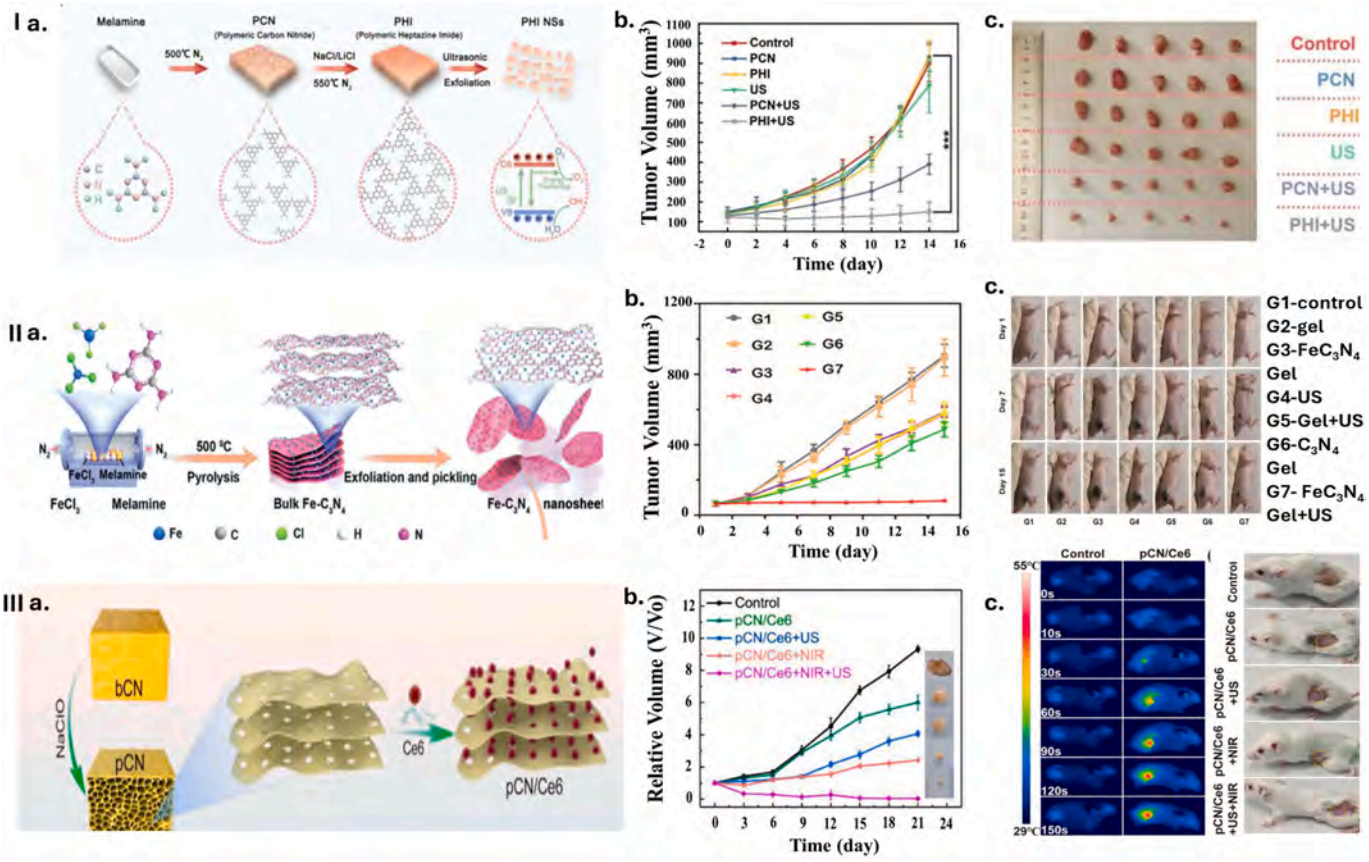

Fig. 1. Schematic illustration of applications of carbon nitride and its derivatives in sonodynamic therapy. I. Polyheptazine imide (PHI) **a.** Preparation of PHI, **b.** Tumor volumes of mice in different treatment groups, **c.** Images displaying tumors from distinct groups at the completion of treatment [94]. Copyright 2024, Wiley. **II.** Iron single atoms doped Carbon Nitride (FeC_3N_4) **a.** Preparation of FeC_3N_4, **b.** Tumor volume growth curves in diverse treatment groups, **c.** Images displaying tumors from distinct groups at day 0, 7 and 15 [90]. Copyright 2023, Wiley. **III.** Protonated 2D carbon nitride (pCN) sensitized with Ce6 **a.** Preparation of pCN/Ce6, **b.** Tumor growth curves and representative images, **c.** Infrared thermal images of the mice (left) and Photographs of mice treated for 21 days (right) [112]. Copyright 2021, Elsevier. Reproduced with permission.

performance but also supported the SDT via decomposition of H_2O_2 as well as GSH depletion. Until now, only 2 typical MXenes including Ti_3C_2 and Nb_2C were employed for biomedical applications. In addition, Ti_3C_2 and Nb_2C also possess high photothermal conversion efficiency that facilitates the amalgamation with photothermal therapy for augmenting therapeutic efficacy synergistically. Table 2 summarizes SDT cancer treatments using MXene-based nanosonosensitizers.

As shown in **Table 2**, 2D MXene-based nanosonosensitisers enabled the synergistic combination of SDT and PTT, owing to their intrinsic piezoelectric properties and high photothermal conversion efficiency. This combined approach demonstrated excellent tumouricidal effects, with tumor growth inhibition rates exceeding 90 %. In some cases, complete eradication of both primary and distant tumors was achieved using very low doses (2–5 mg/kg) of certain 2D MXenes. However, inconsistencies in ultrasound parameters (frequency, intensity, and duration), as well as variations in dosage and treatment timelines, pose challenges in directly comparing therapeutic outcomes across different 2D MXenes. Additionally, diverse modification strategies lead to distinct tumor-targeting mechanisms, which are highly dependent on the intrinsic properties of each material. As such, it remains difficult to determine which modification offers the most effective improvement in treatment outcomes. Fig. 4 exhibits representative utilization of MXenes nanosheets as piezoelectric sonosensitizers.

3.3.2.6. Metal derivatives

3.3.2.6.1. Metal oxides.

– *Titanium oxides*

Pure TiO_2 was usually not adequate for effective SDT due to their relative wide bandgap (3.2 eV) and fast recombination of electron-hole pairs. To improve the sonodynamic performance of TiO_2, introduction of defects and dopants or combination with other materials to construct heterojunction were useful solutions. H-TiO_2 modified with Pd has been synthesized for combinational sono-chemodynamic therapy. The oxygen defects caused by the loading of small amount of Pd narrowed the bandgap of H-TiO_2 that facilitated the easier separation of electron-hole pair under US. Moreover, Pd catalyzed H_2O_2 decomposition into O_2 that not only promoted SDT but also reduced hypoxia level. Ti^{3+} in TiO_2 could be Fenton-catalyzed agent that triggered the production of *OH for CDT. After 14 days of treatment, the significant suppression of tumors growth was observed on mice received SDT/CDT treatment utilized Pd/H-TiO_2 [144]. H-TiO_2/C nanosheets were prepared via the hydrogen reduction of MOF-derived TiO_2/C composite and employed for PTT/CDT/SDT treatment on 4 T1 tumor-bearing mice for 14 days. The significant antitumor effects were observed on treated mice compared to control ones. The nanosheets performed good ROS yield production under US with high photothermal conversion efficiency. Moreover, Ti^{3+} from these sheets could catalyze the decomposition of H_2O_2 to *OH for CDT [145]. Au nanocrystals at size of 5 nm anchored on the edge of TiO_2 nanosheets were synthesized for SDT treatment of MCF-7 tumors for 15 days. The modification Au-TiO_2 nanosheets with triphenylphosphine (TPP) and AS1411 aptamer (Au-TiO_2-A-TPP) was applied for mitochondria and organelle targeting. Au on the edge

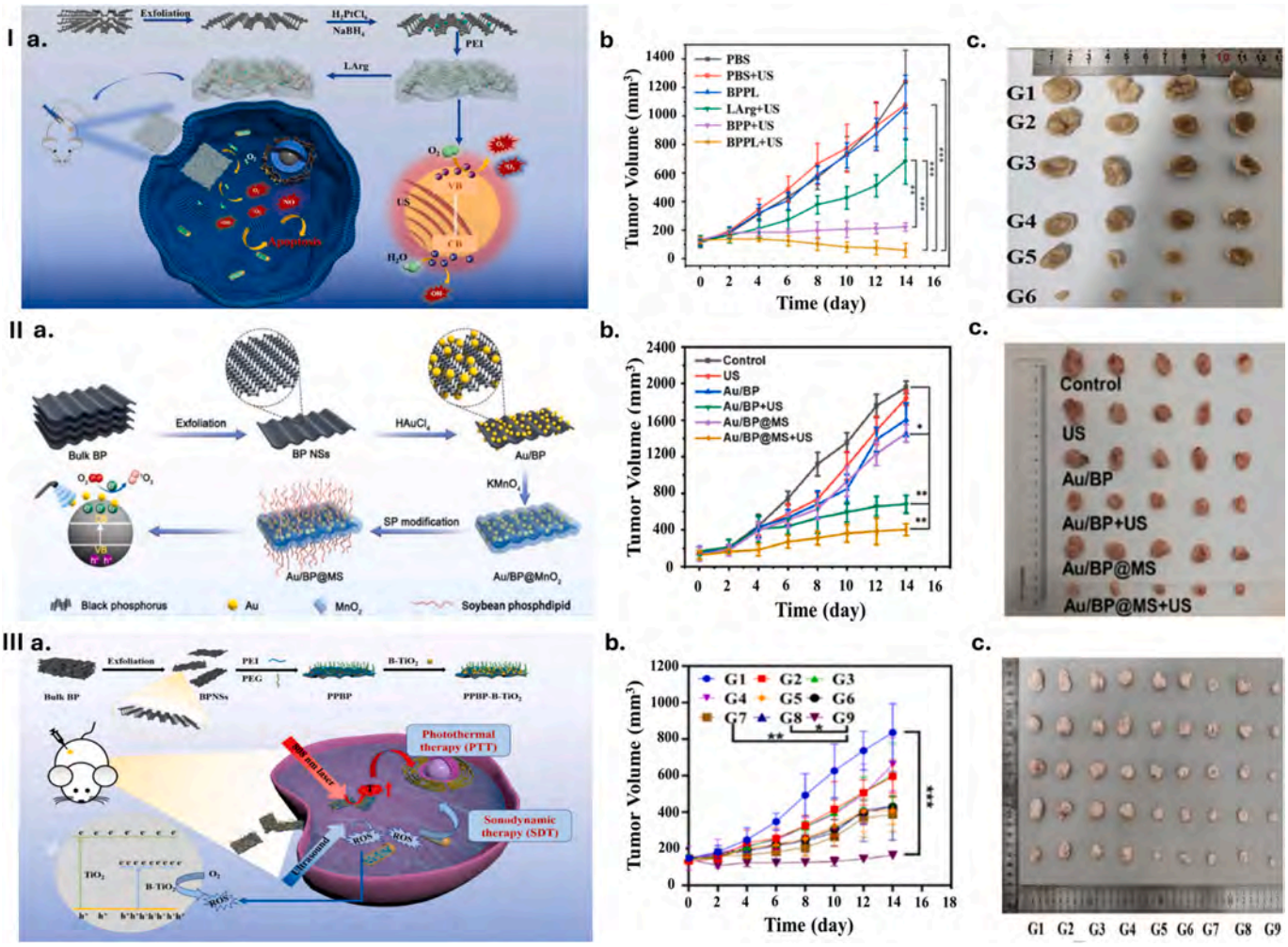

Fig. 2. Schematic illustration of applications of black phosphorus in sonodynamic therapy. I. Pt-modified black phosphorus nanosheets loading with l-arginine (BPPL)**. a.** The fabrication procedure and the anticancer mechanism of BPPL, **b.** Tumor growth curves**, c.** Images of tumors collected from different treatment groups of mice after 14 days, in which G1: PBS group, G2: PBS + US group, G3: BPPL group, G4: LArg + US group, G5: BPP+ US group, G6: BPPL + US group [48]. **II.** Gold/black phosphorus@MnO_2 nanoplatforms (Au/BP@MS)**. a.** Preparation of Au/BP@MS, **b.** Relative tumor volume curves of the mice in each experimental group during treatment, **c.** Representative image of tumors collected from mice groups on day 14 [118]. **III.** Oxygen-deficient titanium dioxide-loaded black phosphorus (B-TiO_2)**. a.** Fabrication of B-TiO_2, **b.** The growth curve of the tumor during the treatment period (14 days), **c.** Photos of tumors in each group after treatments, in which G1: PBS, G2: PPBP, G3: B-TiO_2, G4: PPBP-B-TiO_2, G5: PPBP + L, G6: B-TiO_2 + US, G7: PPBP-B-TiO_2 + L, G8: PPBP-B-TiO_2 + US, G9: PPBP-B-TiO_2 + L + US (L: light, US: ultrasound, PPBP: PEI-PEG-BP) [115]. Copyright 2022, Elsevier. Reproduced with permission. (For interpretation of the references to colour in this figure legend, the reader is referred to the web version of this article.)

promoted the ROS yield via reduction of pure TiO_2 wide band gap (3.20 eV) and delay of charge recombination as electron traps [146]. Cu_2O, a semiconductor with narrow bandgap (2.2 eV), was used to form non-stoichiometric *Z*-scheme heterojunction with TiO_2 ($Cu_{2-x}O$@TiO_{2-y} nanosheets) for the combinational CDT/SDT treatment on 143B tumors for 14 days. When the heterojunction structure formed, the more negative CB of Cu_2O and more positive VB of TiO_2 promoted the more effective $^1O_2$ and *OH generation under US to attain better sonodynamic performance. Moreover, the Cu ion release could not only provide the CDT via catalyzing Fenton reaction but also cause GSH depletion. After CDT/SDT, all 143B tumors were eradicated completely in $Cu_{2-x}O$@TiO_{2-y} treated mice [147]. Trienzyme-like Co_3O_4@TiO_{2-x} exhibited the higher ROS yield compared to TiO_2 owing to enhancement of electron-hole separation. Moreover, both Co_3O_4 and TiO_2 were useful catalysts for Fenton reaction that provided the synergistic CDT/SDT. The combination created heterojunction that boosted the $^1O_2$ and *OH generation 4.6, 4.3 times and 6.7, 12.8 times higher than that of single oxides, respectively. The in vivo tumor ablation result (~100 %) in 143B-tumor bearing mice were significant evidence for excellent antitumor effects of CDT/SDT treatment with Co_3O_4@TiO_{2-x} after 14 days [148]. 2D TiO_2@MnO_{2-x} core/shell heterostructure was fabricated to induce sono-chemodynamic therapy on 4 T1 tumor-bearing mice. Beside boosting sonodynamic effects of TiO_2 nanosheets via facilitating the separation of electron-hole pairs, MnO_{2-x} nanodots anchoring on the surface of TiO_2 also provided GSH depletion, hypoxia alleviation and chemodynamic effects (Fenton) via reactions with GSH and intratumor H_2O_2. The decomposition of H_2O_2 into O_2 was a perfect tool to relieve the tumor microenvironment (TME) as well as supply O_2 source for SDT. Tumor growth suppression reached 79 % in mice treated with TiO_2@MnO_{2-x}-PEG + US compared to 19.4 % and 36.4 % in ones treated with TiO_2@MnO_{2-x}-PEG and TiO_2-PEG + US. This confirmed the benefit provided by combinational SDT/CDT and formation of heterojunction structures between MnO_2 and TiO_2 [149].

– *Non-centrosymmetric oxides*

Many single atoms including Pt, Cu, Fe, Co, and Ni were doped on non-centrosymmetric oxy-vacancy WO_{3-x} nanosheets to generate novel

Table 1
Sonosensitizers based on 2D LDHs and their application SDT cancer treatment.

LDHs	Metal Doping or Modification	Bandgap (CB band)	In Vitro	In Vivo	Dosage	US parameter			Key Results	Mechanism	Ref
						Frequency	Intensity (W/cm^2)	Time (min)			
ZnAl LDHs	Cu	3.607 eV (−1.468 eV)	HUVECs CT26	Both CT26 and 4 T1 tumors bearing mice (5 days)	5 mg/kg,	30 kHz	3	10	– Eradicated tumors after 5 days (~100 %) – 100 % treated mice survived after 60 days	– Cu doped ZnAl LDHs via ion substitute to not only improve SDT but also provide synergistic SDT/cuproptosis. – Cu induced Jahn-Teller effect, lattice distortion and atomic disarrangement. – Cu^{2+} can trigger the GSH depletion and cuproptosis	[125]
CoBiMn-LDHs		1.48 eV (−1.73 eV)	4 T1	4 T1 tumors bearing mice (16 days)	10 mg/kg	40 kHz	3	6	– Suppressed tumors growth and reduced the size (~90 %)	– Mn^{4+} alleviated the TME via H_2O_2 decomposition. – Defects on CoBiMn LDHs improved SDT effectively via narrow the bandgap and enhance electron-hole separation.	[95]
CoFe-LDHs	Bi	1.9 1 eV (−1.06 eV)	4 T1	4 T1 tumor-bearing mice (16 days)	10 mg/kg	40 kHz	3	6	– Completely inhibited the tumor growth – Mice treated with Bi-doped CoFe-LDHs + US survived with 60 days.	– The Bi doping has narrowed the bandgap of CoFe-LDHs from 2.44 to 1.91 eV and inhibited electron-hole pair recombination. That improved the therapeutic efficacy significantly. – Transformation to amorphous has increased the piezoelectric properties – Fe ion could act as MRI contrasting agents.	[126]
CoW-LDHs		1.41 eV (−1.17 eV)	4 T1	4 T1 tumors bearing mice (16 days)	10 mg/kg	40 kHz	3	3	– Suppressed tumors growth and reduced the size (estimate ~98 %) – Survival rate of CoW-LDHs treated mice is 46 days	– The transformation of CoW from crystalline to amorphous has narrowed the bandgap from 2.42 to 1.41 eV and reduced CB band from −0.99 to −1.17 eV that promoted the ROS generation under US	[127]
MnMgAl-LDHs	Mn to MnO_2		CT26	CT26 tumor-bearing mouse (14 days)	40 mg/kg	50 kHz	3	3	– Suppressed growth of both primary tumors (~90 %) and distant tumor (75 %)	– Mn in LDHs has been oxidized to MnO_2 that provided enhancement of SDT/CDT and activation of cGAS/STING by DMXAA/Mn^{2+} – LDHs were not only sonosensitizer but also nanocarrier of DMXAA	[104]
CoW-LDHs			4 T1	4 T1 tumors bearing mice (15 days)	Each mouse 0.1 mL (0.5 mg/mL)	40 kHz	3	3	– Suppressed tumors growth (~69.5 %)	– Loading of YW3–56 (PAD4 inhibitor) allowed synergistic SDT/immunotherapy. – LDHs played the role of sonosensitizer and nano-carrier	[101]
CoMo-LDHs	Mn	1.82 eV (−0.99 eV)	4 T1	4 T1 tumors bearing mice (16 days)	10 mg		2	6	– Suppressed tumors growth and reduced the size (estimate ~98 %)	– Mn doping not only alleviated TME via H_2O_2 decomposition and GSH depletion but also narrowed the bandgap that enhances ROS production.	[128]
CuMgAl LDHs	Pt	1.76 eV	HeLa	HeLa tumors bearing mice (15 days)	10 mg/kg	1 MHz	1	10	– Suppressed tumors growth and reduced the size (~95 %)	– Pt doping facilitated mimicking of Catalase and Oxidase – Cu depleted GSH	[129]

(*continued on next page*)

Table 1 (*continued*)

LDHs	Metal Doping or Modification	Bandgap (CB band)	In Vitro	In Vivo	Dosage	US parameter			Key Results	Mechanism	Ref
						Frequency	Intensity (W/cm^2)	Time (min)			
NiFe-LDHs		2.09 eV (−0.69 eV)	4 T1	4 T1 tumors bearing mice (14 days)	18 mg/kg	1 MHz	1	3	– Completely inhibited the tumors growth (~91.7 %)	– Pt doping reduced the bandgap from 3.70 to 1.76 eV – Under US irradiation, the separation of electron-hole pairs occurred, thereby triggering the $^1O_2$ generation. – Fe ions allowed NiFe to have peroxidase property to produce *OH – Mixed-valence Fe (II)/(III) resulted in the GSH depleting ability	[130]
CoNi-LDHs	Pt		4 T1	4 T1 tumors bearing mice (14 days)	20 mg/kg	1 MHz	1.5	2	– Suppressed tumors growth and reduced size (estimate ~98 %)	– Under US irradiation, Pt-CoNi LDHs released Pt ions and triggered ROS production. – Pt interacted with DNA and trigger DNA damage. This led to activation of cGAS/STING pathway and immune response via enhancing PD-1 inhibitor effects.	[105]
MgFe LDHs	Mn	1.33 eV	4 T1	4 T1 tumors bearing mice (14 days)	10mg/kg	30 kHz		10	– Suppressed tumors growth (~85 %)	– Mn has been used to substitute Mg in MgFe LDHs that narrow the bandgap 0.43 eV and improve sonosensitivity. – Mn ions supported SDT and relieved TME via H_2O_2 decomposition – GSH depletion	[131]

sonosensitizers. Among these single atoms doped nanosheets, Cu-WO_{3-x} exhibited the highest yield in ROS generation for SDT [150]. 4 T1 tumors were quickly eradicated after 10 days of 16-day-SDT treatment using Cu-WO_{3-x}. The doping of metals single atoms narrowed the bandgap of WO_{3-x} notably (from 3.14 eV to ~1.8–1.7 eV) that made electron-hole pair separation in easier way. Moreover, the single atoms could act as electron traps that inhibited the recombination of electron-hole pairs during SDT [150]. Closely contacted Cu_2O-$CoWO_4$ (CCW) nanosheets were developed for combination of photothermal and sonodynamic assisted cuproptosis therapy on 4 T1 tumor-bearing mice for 14 days. The amalgamation of CCW and L-arginine into injectable hydrogel provided 95.1 % tumor inhibition under laser/ultrasound simultaneous irradiation. Besides sonodynamic effects triggered by Cu_2O (E = 1.79 eV, CB = -1.05 eV) and $CoWO_4$ (E = 2.6, CB = -0.933 eV), Cu^+ can be oxidized by endogenous hydrogen peroxide to Cu^{2+} that promoted cuproptosis in cancer cells. L-arginine could be used as NO release compound for gas therapy synergistically [108].

Vanadium vacancy-rich BiVO4 nanosheets were synthesized via facile hydrothermal method and utilized as piezoelectric sonosensitizer (CB = -0.38 eV, VB = 2.13 eV). The vanadium vacancy facilitated ROS production via promoting electron formation under US. Moreover, the introduction of vanadium vacancy could allow peroxidase enzyme mimicking to produce *OH from H_2O_2 depletion of glutathione. These increased the oxidative stress that inhibited the growth of 4 T1 cancer cells. This material also acted as CT contrasting agent that supported the CT imaging combined with CDT/SDT [151]. Bi_4NbO_8Br-polyvinylpyrrolidone (BNOBP) piezoelectric sonosensitizer were used as sonosensitizer due to the relatively narrow bandgap (2.45 eV) compared to the other mono-compounds including TiO_2 (3.20 eV), BiOBr (2.93 eV), and Bi_2MoO_6-PEG (3.04 eV). The strong interactions between Bi—O and Nb—O supported the carrier transfer, and asymmetric structure of BNOBP boosted the electron-hole pairs separation. Moreover, BNOBP also depleted intracellular GSH concentration. During 14 days of SDT treatment, BNOBP successfully inhibited the growth of 4 T1 tumors in mice with GSH consumption rate attained 22.8 % [152]. In another research, 2D Bi_4NbO_8Br (BNB) single crystalline nanosheets composing of $(Bi_2O_2)^{2+}$ layers, $(NbO_4)^{3-}$ wa\ere developed to enhance the separation of charge carriers. Moreover, owning the bandgap of 2.48 eV and CB = -0.98 eV (more negative than −0.33 eV), BNB nanosheets were promising candidate for piezocatalytic ROS generation under US excitation. The VB of BNB (1.5 eV) did not allow it to trigger the production of *OH from water. However, stress induced by US built in piezoelectric field caused internal polarization. This led to the band bending to make VB more positive and permit the redox reaction to from *OH. The complete inhibition was observed on Hepa1–6 tumor-bearing mice after only 7 days under SDT treatment [153]. Bismuth tungstate (Bi_2WO_6) nanosheets that owned the appropriate bandgap (2.6–2.8 eV) were doped with Fe to promote their piezoelectricity via narrowing the bandgap 0.4 eV (CB = -0.51 eV). Under US excitation, these sheets exhibited excellent SDT efficiency on 4 T1 tumor treatments. The existence of Fe ions also generated *OH via Fenton reaction. This facilitated the synergistic CDT/SDT. Tumor growth inhibition attained 68.4 % on mice group treated with Fe-Bi_2WO_6 under US [154]. $Bi_4Ti_3O_{12}$ (BTO) nanosheets were used as excellent sonopiezoelectric-sensitizer for SDT

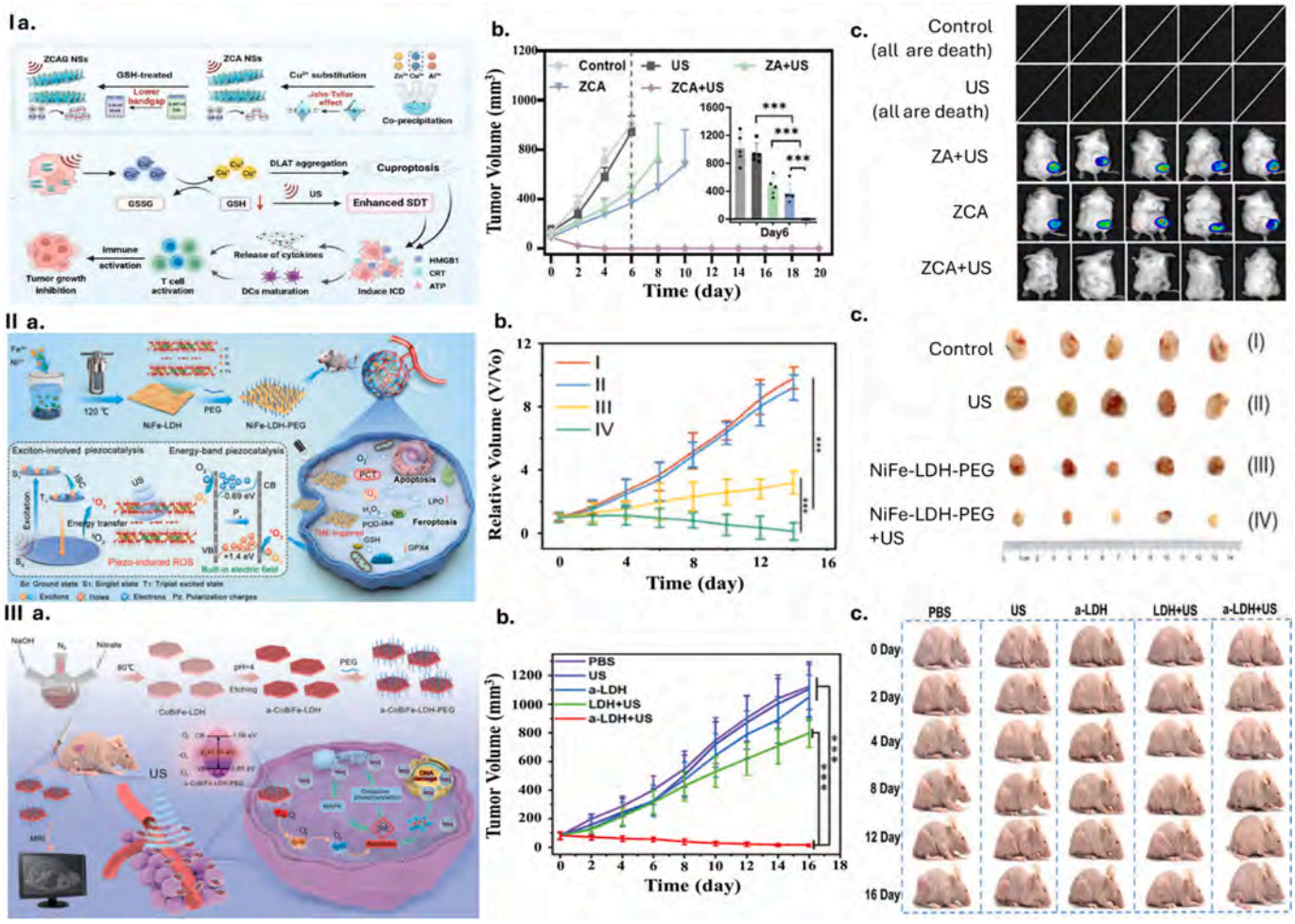

Fig. 3. Schematic illustration of applications of layered double hydroxides (LDHs) in sonodynamic therapy. I. Cu-substituted ZnAl ternary layered double hydroxide nanosheets (ZCA). **a.** Synthetic procedure of ZCA, **b.** Volumes of 4 T1-luc breast cancer tumors treated with the control, US (30 kHz, 10 min), ZA (5 mg/kg, intratumor injection) + US, ZCA, or ZCA + US, **c.** Bioluminescence imaging of each mouse after different treatments on day 20 [125]. Copyright 2024, American Chemical Society. **II.** Bilayered ultrathin NiFe-LDH nanosheets. **a.** Preparation of NiFe-LDH nanosheets and their piezocatalysis mechanism, **b.** Changes in the relative volume of tumors with different treatments, **c.** Representative digital images of 4 T1 tumor-bearing mice with various treatments [130]. Copyright 2024, Wiley. **III.** CoBiFe-LDH-PEG nanosheets. **a.** Preparation of a-CoBiFe-LDH-PEG nanosheets and their application in SDT, **b.** Tumor growth curve of 4 T1 tumor-bearing mice in each group after 16 days of treatment, **c.** Photographs of 4 T1 tumor-bearing mice in each group at day 0, 2, 4, 8, 12, 16 [126]. Copyright 2024, Wiley. Reproduced with permission.

treatment of 4 T1 tumor for 14 days under US excitation. To improve the piezoelectric effects of BTO that led to higher ROS generation yield, the introduction of oxygen vacancy that played electron traps' role and corona polarization that enhanced the charge separation and migration via increase of asymmetry was applied. Not only aggrandize the superoxide anion ($\bullet O^{2-}$) and hydroxyl radical ($\bullet$OH) production, but these sheets could also catalyze the transformation of CO_2 to CO for combination with gas therapy. Killing 85.3 % of cells and significantly suppressing tumors growth under US excitation were striking evidence for the notable sonodynamic antitumor effects of BTO [155]. 2D Bi_2MoO_6 (BMO) nanoribbons, a unique layered structure comprising of $[Bi_2O_2]^{2+}$ units and perovskite-like $[MoO_4]^{2-}$ slabs, were synthesized via a hydrothermal process and employed as a new sonosensitizer. Reacting with intracellular GSH, Mo^{6+} was reduced to Mo^{5+} that led to the generation of oxygen-deficient sites, electron traps, that improved sonodynamic performance. The GSH activation narrowed the bandgap of BMO from 2.73 to 2.38 eV with more negative CB (−0.59 eV) compared to −0.31 eV of pure BMO. This facilitated easier separation of charges. Excellent tumor inhibition (96.6 %) was observed in U14 tumor-bearing mice treated BMO under US irradiation after 15 days [84]. Heterojunctions based on combination of Bi_2MoO_6 (BMO) nanosheets and MXene nanosheets were fabricated for novel therapeutic modalities - SDT-based ferroptosis immunotherapy. The interface between BMO and MXene acted as Schottky barriers in which the electrons from BMO were transferred to MXene to balance Fermi energy levels. This restrained recombination of e − and h + pairs; thus promoted ROS production rate under US excitation. The bandgap of these sheets was 2.67 eV in which CB = -0.98 eV and VB = 1.69 eV. Exogenous US applications triggered the ROS generation of BMO-MXene that boosted ferroptosis and improved the immune response via inducing ICD. These sheets significantly suppressed ID8 proliferation by more than 90 %, triggered lipid peroxidation, abated mitochondrial-membrane potential, and blocked the glutathione peroxidase and cystathionine transporter protein system. The in vivo models with ovarian cancer ID8 cell-bearing mice proved excellent antitumor effects of novel therapeutic strategy with BMO-MXene after 22 days [103].

In another approach, nanoheterojunction constructed via combination of Au nanorods (NRs) and Bi_2O_3 nanoflowers (arrangements of many sheets) (ABO) were synthesized to narrow the naturally wide bandgap of Bi_2O_3 (3.75 to 3.45 eV) that favored its piezoelectric performance for SDT. The presence of Au NRs not only improved the separation of charges but also contributed positively to therapeutic

Table 2
Sonosensitizers based on 2D MXenes and their application in SDT cancer treatment.

MXenes	Modification	Bandgap (CB band)	In Vitro	In Vivo	Dosage	US parameter			Results	Mechanism	Ref
						Frequency	Intensity (W/cm^2)	Time (min)			
$Ti_3C_2T_x$	N doped carbon dots	$Ti_3C_2T_x$ (−0.49 eV)) N-Cdots (−0.63 eV)	4 T1	4 T1 tumor-bearing mice (14 days)	5 mg/kg	50 kHz	3	5	– Completely inhibited tumors growth (~100 %)	– Decoration of C dots promoted ROS production via supporting carrier transfer and preventing electron-hole recombination – The combination of 2 materials allowed the synergistic SDT/PTT.	[138]
Ti_3C_2	Oxygen defects		4 T1	4 T1 tumor-bearing mice (14 days)	20 mg/kg	40 kHz	3	15	– Completely inhibited tumors growth (~100%)	– Oxygen defects on surface formed TiO_2/Ti_3C_2 that not only promote the separation of e − and h + but also capture electronic to prevent the recombination via oxygen vacancy. – This modification also allowed the synergistic SDT/PTT	[139]
Ti_3C_2	CuO_2@BSA		U87 glioma cells	U87 tumor-bearing mice (14 days)	10 mg/kg	1 MHz	2	3	– Inhibited tumors growth significantly (~93 %)	– CuO_2 released Cu^{2+} under TME that not only depleted GSH but also triggered CDT – Ti_3C_2 was in situ oxidized into TiO_2 under presence of H_2O_2 that formed TiO_2/Ti_3C_2. This nanosonosensitizer systems augmented SDT efficacy via enhancement of electrons-holes separations.	[135]
Ti_3C_2	Pd (Ti vacancies)		4 T1	4 T1 tumor-bearing mice (14 days)	4 mg/kg	50 kHz	2	5	– Completely eradicated primary tumor (100%) – Suppressed significantly distant tumor – Treated mice survived after 50 days	– Pd atoms were introduced into Ti vacancies of $Ti_{3-x}C_2T_y$ nanosheets to dramatically augment sonodynamic performance. Pd atoms not only acted as electron traps to restrain electron–hole recombination but also mimicked catalase to decompose H_2O_2 into O_2 supporting SDT efficiency. – Holes in the VB of $Ti_{3-x}C_2T_y$ could deplete overexpressed GSH. – These sheets induced ICD to stimulate systemic immune responses for SDT-immunotherapy.	[97]
Ti_3C_2	TiO_2	2.37 eV	4 T1	4 T1 tumor-bearing mice (14 days)	20 mg/kg	1 MHz	1.5	10	– Suppressed tumor development significantly (in 2/5 mice, tumors were eradicated)	– TiO_2/Ti_3C_2 was manufactured via regulated dissolved-oxygen concentration with Ar – This modification has narrowed the bandgap and prevented the recombination of electron-hole pairs. – This material also provided the combinational SDT/PTT	[140]
Nb_2C	Schottky junction via niobium oxide	2.5 eV	4 T1	4 T1 tumor-bearing mice (14 days)	20 mg/kg	1 MHz	1.5	–	– Inhibited tumors growth and reduced tumors size (96.32 %)	– The modification of Nb_2C formed Nb_2O_5/Nb_2C heterojunction augmented ROS generation efficiency.	[141]

(*continued on next page*)

Table 2 (*continued*)

MXenes	Modification	Bandgap (CB band)	In Vitro	In Vivo	Dosage	US parameter			Results	Mechanism	Ref
						Frequency	Intensity (W/cm^2)	Time (min)			
Nb_2C	polythiophene		4 T1	4 T1 tumor-bearing mice (14 days)	200 μL (200 μg/mL	1 MHz	1.5	10	– Inhibited tumor growth considerably	– The modification also supported therapeutic effects via combination of SDT/PTT – Nb_2C could mimic Catalase via O_2 generation from H_2O_2 that enhanced SDT – Polythiophene played as sonosensitizers	[142]
Ti_3C_2	Pt		4 T1	4 T1 tumor-bearing mice (20 days)	2 mg/kg	3 MHz	1	2	– Effectively eliminated primary and abscopal tumors (~100%) – No mice death in treated group for 40 days	– Pt deposited on Ti_3C_2 formed heterojunctions to improve sonodynamic effects. – Ti_3C_2 possessed photothermal property that allowed the combination between SDT and PTT – Pt could decompose H_2O_2 into O_2 that supplied oxygen for SDT as well as alleviated hypoxia.	[137]
Ti_3C_2	TiO_{2-x}	2.65 eV	4 T1	4 T1 tumor-bearing mice (14 days)	20 mg/kg	1 MHz	1	5	– Eradicated tumors in almost mice (4/5)	– Modification of Ti_3C_2 with TiO_{2-x} narrowed the bandgap from 3.32 to 2.65 eV and inhibited the recombination of electron-hole pairs via electron traps – The combination of 2 titanium compounds also allowed synergistic photo-sono theranostic.	[143]
Ti_3C_2	atomic-thin chitosan-exfoliated MoS_2 (ch-MS)	1.84 eV (−1.1 eV)	4 T1	4 T1 tumor-bearing mice (20 days)	2 mg/kg	1.07 MHz	0.309	–	– Significantly inhibited tumor growth (tumors disappeared in 3 of 5 SDT/PTT treated mice)	– The heterojunction via interface of Ti_3C_2 and MoS_2 led to the formation of Schottky barrier that enhanced separation and restrained recombination of electron-hole pair. – Ti_3C_2 allowed the combination between SDT and PTT due to its outstanding photothermal conversion efficiency	[136]

outcomes via photothermal effects. Additionally, Bi_2O_3 could reduce the GSH concentration to disrupt redox balance. The synergistic SDT/PTT therapy inhibited both the tumors growth and metastasis of 4 T1 tumors (primary and distant ones) after 14 days [156]. Ternary *Z*-scheme Bi_2WO_6/TiO_2 − Pt heterojunction ensured effective separations under US excitation via direct transfers and Schottky barriers. Pt could provide peroxidase-catalase property that catalyzed the decomposition of H_2O_2 into O_2 and radicals. This could prevent TME negative effects on SDT treatment and supply source for ROS generation. MB49 tumors treated with Bi_2WO_6/TiO_2 − Pt and US were significantly suppressed after 14 days [157].

A heterojunction structure based on thermally treated natural sphalerite nanosheets (NSH700 NSs) was prepared via calcination and applied for SDT due to its piezo-catalytic effects. Via calcination, NHS nanosheets were deformed to $ZnS/ZnFe_2O_4/ZnO$ nanosheets in which ZnO and ZnS were piezoelectric catalysts and $ZnFe_2O_4$ was photocatalyst. Under 650 nm light and US excitation, NSH700 NSs performed ROS burst to kill MCF-7 cancer cells. The tumors size was successfully suppressed after 15 days of photo-sonodynamic therapy. The redistribution of surface electrons and holes between heterojunction structure could restrain the recombination that allowed more effective ROS generation [158].

Ultrathin-FeOOH-coated MnO_2 nanospheres were synthesized and applied as multifunctional materials for not only the SDT but also TME alleviation via hypoxia relief, H_2O_2 consumption and Glutathione depletion. The presence of ultrathin FeOOH nanosheets allowed the high yield of not only singlet oxygen (1O2) via piezoelectric effects but also hydroxyl radicals (*OH) via catalyzing Fenton reaction. The decomposition of H_2O_2 to O_2 catalyzed by MnO_2 supplied oxygen source for transformation to singlet oxygen under US and broke the TME equilibrium via hypoxia level and GSH reduction. After 21 days of CDT/SDT treatment, MBA-MD-231 tumor on mice were suppressed completely

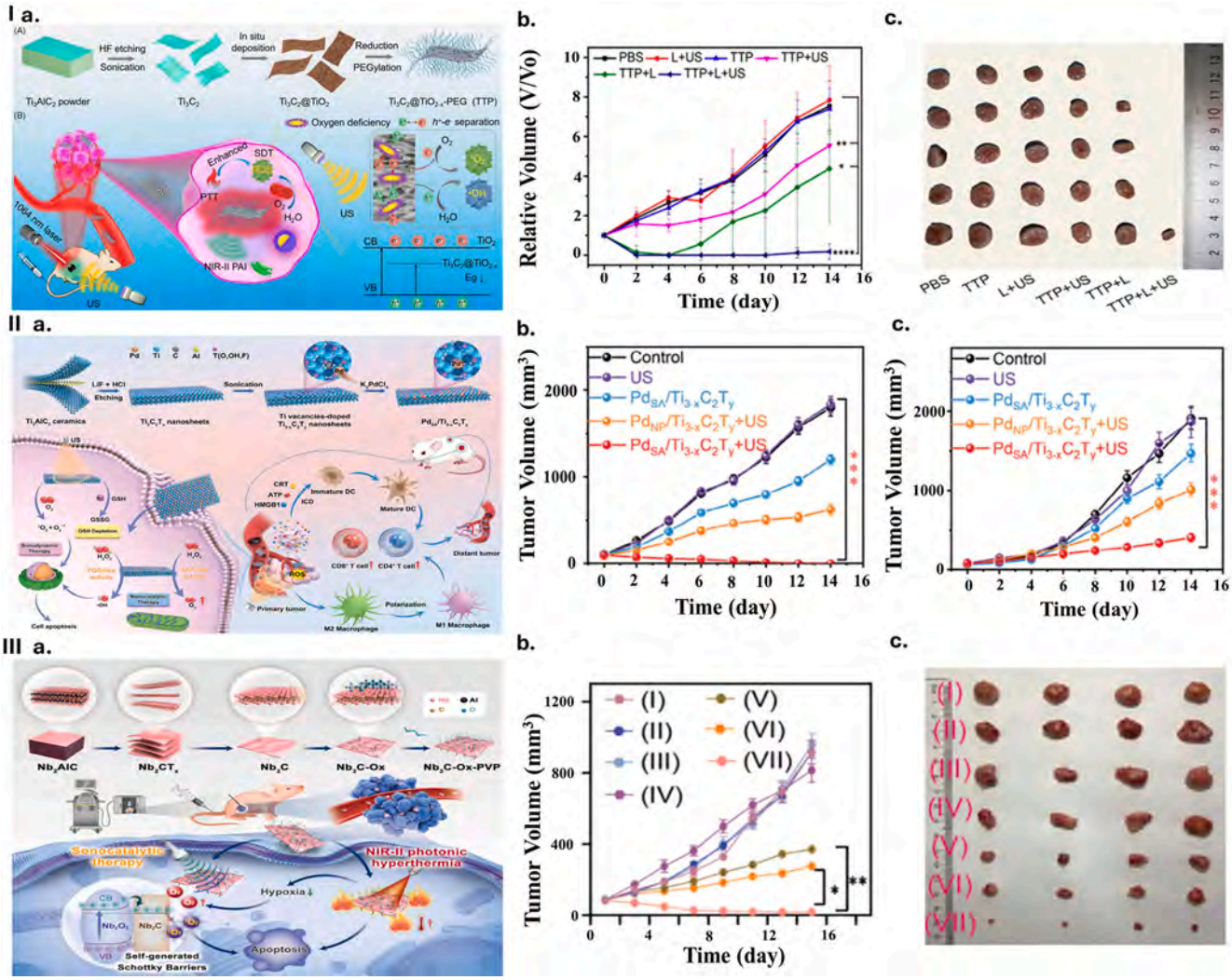

Fig. 4. Schematic illustration of applications of MXenes in sonodynamic therapy. I. In-situ TiO_{2-x} decoration of titanium carbide MXene. **a.** Synthetic procedure of TiO_{2-x} decoration of titanium carbide (TTP), **b.** Relative change in tumor volume after diferent treatments, **c.** The digital images of tumors collected from different indicated groups at 14th day [143]. Copyright 2022, BioMed Central. **II.** Pd single atoms doped $Ti_{3-x}C_2T_y$. (Pd_{SA}/ $Ti_{3-x}C_2T_y$) **a.** Preparation of the $Pd_{SA}/Ti_{3-x}C_2T_y$ and its application for enhanced sono-immunotherapy, **b.** Primary and **c.** distant tumor volume in mice after different treatments [97]. Copyright 2024, Wiley. **III.** Self-generated Schottky barriers in niobium carbide (Nb_2C-Ox). **a.** Construction of Nb_2C-Ox nanosheets, **b.** Tumor growth curves and **c.** Photograph of tumors from 4 T1-bearing mice after different treatments in which (I) Control; (II) Nb_2C-Ox (N); (III): Laser; (IV): US; (V): Nb_2C-Ox + laser; (VI): Nb_2C-Ox + US; (VII): Nb_2C-Ox + laser + US [141]. Copyright 2023, Elsevier. Reproduced with permission.

[159].

3.3.2.6.2. Metal sulfides. 2D metal sulfides belonged to transition-metal dichalcogenide groups (TMD) possessed remarkable piezoelectric property due to the broken inversion symmetry [160]. TMDs usually have 2 phases including 2H which are related to semiconducting phase with trigonal prismatic crystal structure, and 1 T/1 T' which is related to metallic phase with octahedral coordination crystal structure [161,162]. However, the main barriers of this semiconductor class are slow transfer and short recombination time of electron-hole pairs [163]. The doping or surface modification with vacancies are promising solutions to enhance piezoelectrical property that promotes ROS generation under US excitation. Compared to bulk form, the piezoelectric performance of TMD metal sulfides was aggrandized when they were dispatched into layers, especially odd number layers due to the break of inversion symmetry [164]. In addition, sulfur element in metal sulfides could be released as H_2S due to acidity of tumor microenvironment. That allowed the combinational modality between SDT and gas therapy to achieve better therapeutic outcomes. Metal dopants could contribute to amplification of tumoricidal performance via catalyzing the Fenton reaction for chemodynamic effects. Table 3 summarizes metals sulfide-based nanosonosensitizers.

3.3.2.6.3. Metals oxychloride. BiOCl nanosheets had a specific non-centrosymmetric structure due to the presence of Bi^{3+} ions and lone pairs of electrons. Moreover, $(Bi_2O_2)^{2+}$ layer settled between double Cl-layers in the crystal resulted in a built-in electric field that was favorable for electron-hole pairs separation [168]. This contributed significantly to piezoelectric performance of BiOCl. The oxygen vacancies were introduced on the surface of BiOCl (bismuth oxychloride) to not only create charge traps that inhibited the recombination of electron-hole pairs but also diminished the bandgap from 3.10 to 2.61 eV. Therefore, the piezoelectricity of BiOCl waswere promoted in noticeable way. The doping of copper ion not only had the same purpose as oxygen vacancies but also allowed the synergistic CDT/SDT via Fenton like reaction to generate *OH. The CB band of Cu-BiOCl was −1.55ev that provided the significant singlet oxygen production under ultrasound. 4 T1 tumor-bearing mice received CDT/SDT treatment utilized Cu-BiOCl had the complete inhibition on tumor development [91]. L-Buthionine-Sulfoximine (BSO) loaded on sonosensitizer black BiOCl nanosheets (Eg = 2.40 eV) were prepared for amplification of SDT. Under US irradiation, sonosensitizer BiOCl triggered the singlet oxygen generation

Table 3
Metals sulfide nanosonosensitizers and their SDT therapeutic effects.

Metal Sulfides	Modification	Surface modification	Dosage	US parameters			In Vivo Results	Mechanism	Ref
				Frequency	Intensity (W/cm^2)	Time (min)			
TiS_x		DSPE-PEG	5 mg/kg	30 kHz	3	15	– 4 T1 tumor bearing mice (15 days) – Tumor inhibition rate nearly 100 %	– Under TME, TiS_x decomposed and released H_2S for gas therapy – The release of H_2S resulted in Sulfur vacancies and formation of TiO_x that significantly improved sonodynamic performance. – H_2S release not only allowed gas/SDT multitherapy but also triggered immune system to inhibit metastasis	[19]
TiS_2	Mn	DSPE-PEG-NH_2	2 mg/kg	30 kHz	3	10	– CT26 tumor-bearing mice (21 days) – Tumor growth suppression (~87 %) after 10 days	– $MnTiS_2$ could cause sonodynamic effects and H_2S release simultaneously that allowed the combinational gas/SDT. – Mn^{2+} release due to TME promoted DCs maturation and enhanced immune response.	[165]
MoS_2	S (vacancies)		20 mg/kg	1 MHz	1.5	5	– 4 T1 tumor bearing mice (18 days) – Tumor growth suppression (85.4 %)	– MoS_2 nanoflower (many sheets) – Sulfur vacancies were applied to improve piezoelectric property via increasing charge carrier separation and aggrandized ROS generation	[83]
SnS_{2-x}	Cu	PEG	20 mg/kg	1 MHz	1.5	6	– 4 T1 tumor bearing mice (14 days) – Tumor growth suppression (89 %)	– Heterovalent substitution of Sn^{4+} by Cu^{2+}had significant effects on piezoelectrical property of SnS including narrowing the band gap (2.16 to 1.62 eV), promoting the separation of e^-–h^+ pairs, and prolonging recombination time. – Cu^{2+} allowed the CDT/SDT beside the GSH depletion	[163]
WS_2		PEG	25 mg/kg	1 MHz	0.5	3	– MCF-tumor bearing mice (14 days) – Complete suppression (estimate ~90 %)	– CB = -0.76 eV that facilitated singlet oxygen production under US – Triphenylphosphonium (TPP) was modified on surface for mitochondria targeting	[166]
VS_2	Fe	PEG	7.5 mg/kg	40 kHz	6.5	10	– 4 T1-tumor bearing mice (14 days) – Tumor growth suppression (estimate ~60 %)	– Doping with Fe improved SDT effect via prolonging the recombination time of electron-hole pairs – Fe catalyzed Fenton reaction that allowed CDT/SDT	[167]

that not only provided SDT treatment but also contributed to the quick release of glutathione inhibitor BSO to enhance intratumor oxidative stress. This material showed the positive tumor-suppressed effects on 4 T1 tumor bearing mice after 14 days [91]. Iron doped rich oxygen vacancies BiOCl nanosheets offered high ROS generation ability with excellent biocompatibility and colloidal stability. The iron doping and oxygen vacancies had enhanced effects on BiOCl piezoelectric properties via providing extra electron trapping sites. Moreover, the presence of iron could allow the chemodynamic therapy. After 12 days being treated with CDT/SDT using Fe-BiOCl, 4 T1 tumors growth was suppressed considerably [169]. Piezoelectric nanoplatform was fabricated via combination of MnOx, a multi enzyme-mimicked compounds, and BiOCl, piezoelectric material, to act as 2D sonosensitizer for SDT treatment of 4 T1 tumors. MnO_x not only mimicked peroxidase and catalase to produce *OH and O_2 from H_2O_2 but also downregulated GSH concentration. This promoted SDT in a more effective way via supplying oxygen source and radicals' generation. Tumor suppression up to 70 % was performed on 4 T1 tumor bearing mice via SDT [170].

A 2D interplanar heterojunction FeOCl/FeOOH was developed for SDT type I instead of type II. Under US excitation, electrons on the CB of FeOCl were combined with the holes on the VB of FeOOH that create stronger reduction/oxidation potentials of separated electrons on the CB of FeOOH and holes on the VB of FeOCl. The holes on the VB of FeOCl reacted with H_2O to produce O_2 that was immediately and directly reduced to H_2O_2 by the electrons on the CB of FeOOH. Finally, OH generation via this multipath process allowed specific type I SDT. The in vivo therapeutic experiments on MCF-& tumor bearing mice performed the substantially antitumor effects of FeOCl/FeOOH after 14 days [171]. Virtually, SDT processes related to generation of singlet oxygen from oxygen source (Type II).

3.3.2.6.4. Other metals compounds. Bismuth telluride (Bi_2Te_3) deposited with large number of Au on the surface were fabricated and applied as peroxidase like enzyme-sonosensitizer for Hepa1–6 hepatocellular carcinoma mouse treatment under US irradiation. Bi_2Te_3 nanosheets were recognized not only as a peroxidase like enzyme but also as promising sonosensitizer due to their bandgap of 2.34 eV in which CB = -0.56 eV. This enabled US driven piezoelectrocatalytic ROS production via water splitting into H_2 and H_2O_2 [172]. Owning the narrower bandgap (2.50 eV) compared to TiO_2 nanoparticles, TiB_2 nanosheets exhibited much better ROS production under US excitation. To improve the biocompatibility and blood-brain barrier penetrating, TiB_2 nanosheets were encapsulated in RGD peptide modified - macrophage cell membranes. Under simultaneous excitation of US and NIR, TiB_2 allowed the synergistic PTT/SDT via thermoplasmonic effect and ROS generation. U87 tumor-bearing BALB/c nude mice were utilized for in vivo investigations that showed complete inhibition of tumor

development by TiB_2 after 20 days [173]. A liquid-phase exfoliated 2D stanene nanosheets (SnNSs) that were fabricated by the epitaxial growth on various substrates were employed as novel sonosensitizer. Due to the photothermal conversion efficiency of 37.9 %, these sheets also offered photothermal effects beside sonodynamic ones. Owing to the relatively narrow bandgap of 2.3 eV, SnNSs performed good ROS generation including both $^1O_2$ and *OH under US irradiation. 808 nm NIR laser illumination for 8 min could increase the temperature rapidly to 55 °C. Owing to the large surface modified with poly (ethylene glycol), these sheets were ideal nanocarrier for β-elemene anticancer drug. This combinational SDT/CT/PTT treatment for 14 days completely eradicated H1299 tumors in mice via multi-attack mechanism [174]. The first time 2D metal phosphorus trichalcogenides $FePS_3$ was reported as efficient sonosensitizer for synergistic SDT/CDT therapy. These nanosheets had a relatively narrow bandgap of 1.08 eV that allowed the easier US-induced electron-hole pairs separation to trigger the ROS production. Fe^{2+} in $FePS_3$ could react with overexpressed H_2O_2 via Fenton reaction that not only produced *OH radicals for CDT but also formed Fe^{3+} for GSH depletion. These promoted intracellular oxidative stress that led to enhanced apoptosis. After 14 days SDT/CDT treatment, the best tumor inhibition rate of 73.0 % was observed in 4 T1 tumor-bearing mice injected with $FePS_3$. The mono CDT treatment with these sheets (no ultrasound) only gained the tumor inhibition rate is about 19.6 %. To improve dispersity and biocompatibility, lipoic acid-polyethylene glycol (LA-PEG) was modified on the sheet's surface [175]. Figs. 5 and 6 presents recent efforts in using metal compounds to mediate SDT.

3.3.2.7. Metal organic frameworks (MOFs). Unlike the aforementioned sonosensitizers, which activated sonodynamic performance through the piezoelectric effects, MOF-based sonosensitizers could exhibit their sono-activatable properties due to their semiconductivity or the sonosensitizers-ligands presented in their structures. These ligands relied on sonoluminescence to gain ROS generation. Some MOFs had high porosity and low-symmetry crystal structure [176] that facilitated a very low dielectric permittivity [177]. These allowed piezoelectric properties [178]. The metal ions or clusters in their structures could also act as promoters for SDT via decomposition of hydrogen peroxide, Fenton reaction and TME amelioration. Wide range of MOFs with different shapes were used in SDT not only as sonosensitizers but also as nanocarrier due to their specific structures and properties. In this review, we focused merely on 2D MOFs that were sono-activated compounds for cancer therapy. Table 4 summarizes 2D MOFs sonosensitizers and their applications in cancer treatments. In this table, the first four MOFs exhibit sonodynamic effects through piezoelectric properties (via bandgap mechanisms), while the last four demonstrate sonoluminescent properties attributed to their organic ligands.

3.3.2.8. Covalent organic frameworks (COFs). 4,4′,4″,4‴-(ethene-

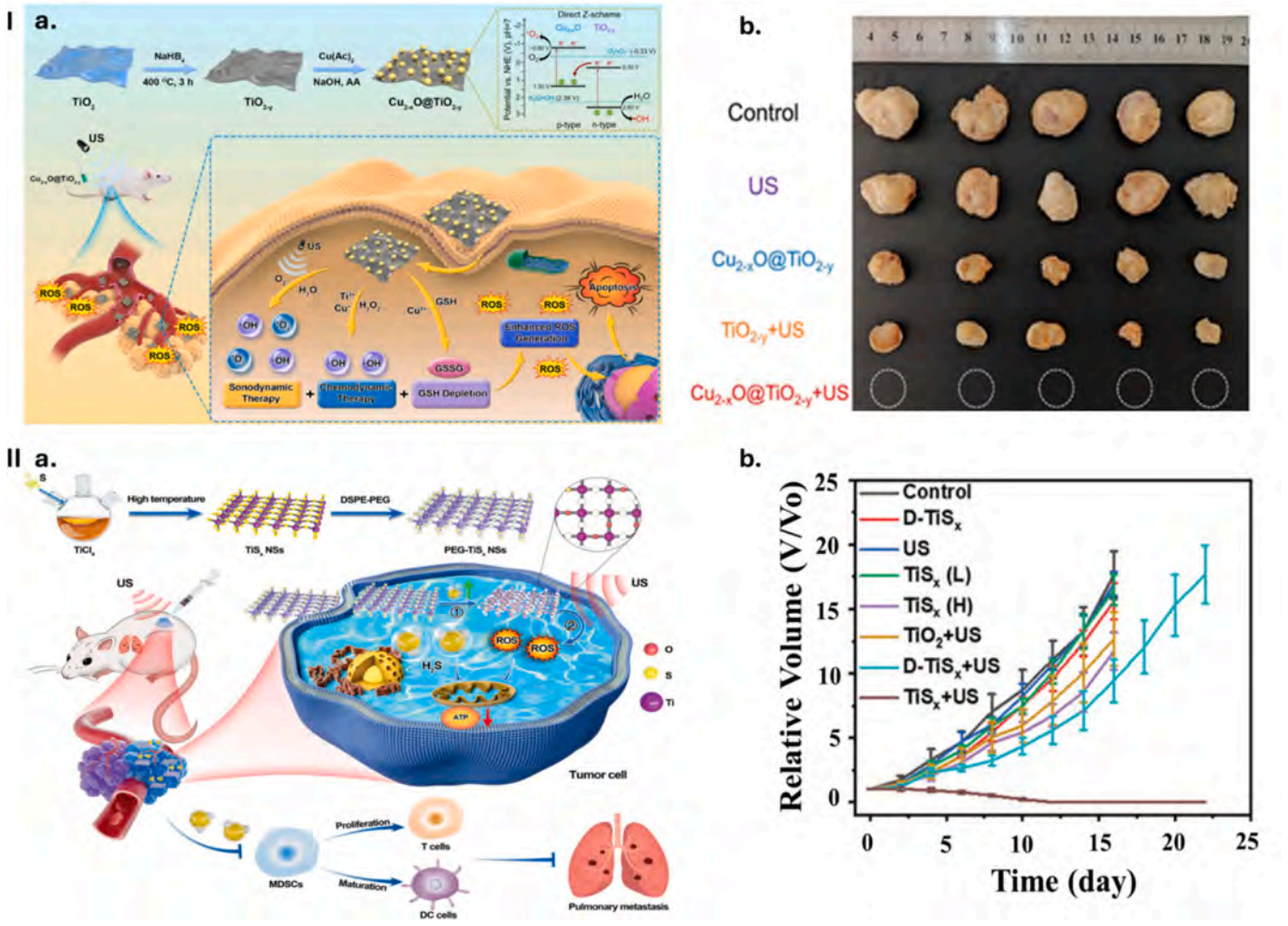

Fig. 5. Schematic illustration of applications of metal oxides and metal sulfides compounds in sonodynamic therapy. I. $Cu_{2-x}O@TiO_{2-y}$ *Z*-scheme heterojunctions. **a.** Synthetic procedure of $Cu_{2-x}O@TiO_{2-y}$**, b.** Representative photographs of tumors after CDT enhanced SDT via $Cu_{2-x}O@TiO_{2-y}$ [147]. Copyright 2022, Elsevier. **II.** TiS_x nanosheets. **a.** Preparation of TiS_x and its application as a cascade bioreactor for H_2S-mediated programmed gas–sonodynamic cancer therapy, **b.** The relative tumor volume in mice with various treatments [19]. Copyright 2022, Wiley.

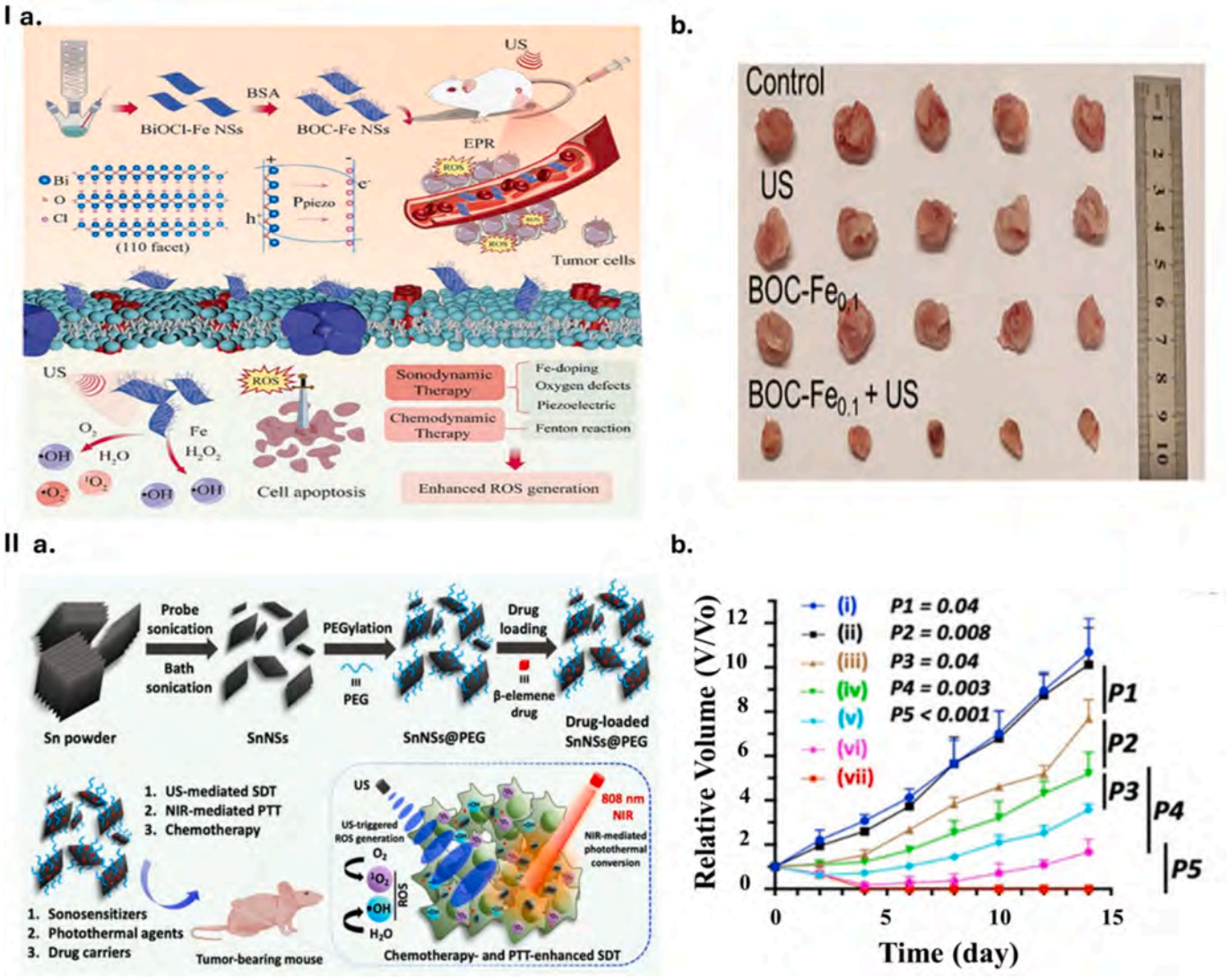

Fig. 6. Schematic illustration of applications of metal oxychloride and other metal compounds in sonodynamic therapy. I. 2D Ultrathin Iron Doped Bismuth Oxychloride Nanosheets (Fe-BiOCl). **a.** Construction of Fe-BiOCl nanosheets, **b.** Photo of tumors dissected from mice at 14 d after different treatments [169]. Copyright 2023, Wiley. **II.** Polyethyleneglycol functionalized stanene-based nano-sheets (SnNSs@PEG). **a.** Preparation of SnNSs@PEG and its application for chemotherapy- and photothermal therapy (PTT)-enhanced sonodynamic therapy (SDT) **b.** Average tumor growth curves for 14 days after various treatments, in which (i) control, (ii) NIR + US, (iii) β-elemene (E), (iv) SnNSs@PEG-E, (v) SnNSs@PEG-E + US, (vi) SnNSs@PEG-E + NIR, (vii) SnNSs@PEG-E + NIR + US [174]. Copyright 2021, Wiley. Reproduced with permission.

1,1,2,2-tetrayl) tetrabenzaldehyde (L-TPE) and N, N,N′,N′-tetrakis (4-aminophenyl)-1,4-phenylenediamine (*L*−NN) could not generate ROS under US if they stayed alone. However, when they were combined to create COF via imine linkages, this COF owned intrinsic sonodynamic effects. To enhance ROS generation, copper ions were incorporated. Moreover, the presence of copper ions not only amplified prominent sono-triggered singlet oxygen production but also reacted with endogenous H_2O_2 to form *OH radicals. That allowed the combinational SDT/CDT. The in vivo studies on 4 T1 tumor-bearing mice for 13 days exhibited promising antitumor effects of this Cu-COF via a synergistic SDT/CDT. The tumors were eradicated completely on 2/5 mice while the other ones had significant size reduction [186]. Inorganic/organic COF heterojunctions nanosheets were fabricated by in situ growth of COF of 1,3,5-tris(4-aminophenyl) benzene (TAPB) and terephthaldehydes on surface of ultrathin bismuth oxycarbonate $Bi_2O_2CO_3$ nanosheets (B-NSs). The anchoring of COFs on the surface reduced the bandgap of B-NSs from 3.05 eV to 2.06 eV that promoted the separation and minimized recombination of electron-hole pairs. This led to the enhancement of ROS production under US. 14-days during SDT treatment with COF-B-NSs suppressed completely the tumor development in 4 T1 tumor-bearing mice [187]. Fig. 7 summarizes recent applications of MOFs and COFs in SDT.

3.3.2.9. The other compounds. Hydroxy-functionalized 2D boron (B-OH NSs) could activate piezocatalytic ROS generation under US irradiation due to their relatively narrow bandgap (~2.23 eV). After 14 days of SDT treatment, 4 T1 tumor-bearing mice intravenously injected with B-OH had the striking suppression of tumor growth. Moreover, B-OH nanosheets could mimic the peroxidase enzyme to trigger the generation of *OH radical that supported SDT in a more effective way [188].

L-cysteine-iodine (l-Cys-I) nanosheets were fabricated via self-assembly between L-cysteine and Iodine by conjugation at coordination site. These nanosheets were anchored with DOX on surface for combinational chemo/sonodynamic therapy. Moreover, the existence of iodine promoted CT imaging. Under US excitation, these nanosheets accelerated the singlet oxygen production and released the DOX. MCF-7 tumor-bearing mice treated with L-cysteine-iodine nanosheets under US had the significant tumor growth inhibition (up to 92.4 %). The

Table 4
2D MOFs sonosensitizers and their cancer treatments applications.

MOFs	Metals	Ligands	Eg (CB)	Cell types	Dosage	US parameter			In Vivo Results	Mechanism	Ref
						Frequency	Intensity (W/cm^2)	Time (min)			
Piezoelectric MOFs											
ZnAl-TCPP	Zn and Al	meso-tetra(4-carboxyphenyl) porphine (TCPP)	1.9 eV	4 T1	10 mg/kg	40 kHz	3	5	– Significantly inhibited tumor growth after 16 days (estimate >95 %) – 100 % mice treated with ZnAl-TCPP under light + ultrasound irradiation survived after 60 days	– TCPP was organic sonosensitizer that acted as ligand – ZnAl:TCPP = 1:4 performed the best ROS yield under US excitation – These sheets not only exhibited significantly better singlet oxygen production compared to TCPP and ZnAl under US but also allowed PDT/SDT synergistic therapy.	[179]
Mn-Ti bimetallic MOFs	Mn and Ti	2-aminoterephthalic acid	2.7 eV	4 T1	20 mg/kg	1 MHz	1	6	– Completely inhibited tumor growth after 15 days (estimate >95 %, 1/5 tumor disappeared in treated group).	– Mn-Ti MOFs had non-centrosymmetric and suitable bandgap for piezoelectric effects under US excitation that triggered ROS generation. – High piezovoltage up to 2.9 V that could overcome bandgap barrier that not only promoted the electron-hole pairs separation to produce ROS but also caused depolarization of mitochondrial and plasma membrane	[180]
Cu-2MI	Cu	2-methylimidazole (2-MI)	2.75 eV (−0.77 eV)	4 T1	100 μL (2 mg/mL) each mouse;	1 MHz	1	4	– Strongly suppressed tumor growth after 14 days (~90 %).	– Cu-2MI had the appropriate energy bands for sono-piezoelectric ROS generation. – Cu^{2+} in MOFs could react with GSH and H_2O_2 that provided GSH depletion as well as CDT via catalyzing Fenton reaction. – Cu^{2+} also contributed to cuproptosis.	[181]
Mn-TCPP	Mn	Tetrakis (4-carboxyphenyl) porphyrins (TCPP) + Gd^{3+}	1.28 eV	CT26	3 mg/kg	1 MHz	1	5	– Significant inhibited tumor growth after 13 days (estimate ~89 %)	– Mn (II) chelating has narrowed the bandgap from 2.7 to 1.28 eV that facilitated ROS generation under US and promoted the charge transfer. – Mn (II) could trigger the Fenton reaction for CDT and enhanced MR imaging.	[182]
Sonoluminescence MOFs											
TBP@MOL	Hf and Ir	5,10,15,20-tetra(p-benzoato) porphyrin (TBP)		CT26 and 4 T1	TBP dose of 0.2 μmole each mouse;	3.4 MHz	2	10	– Strongly suppressed tumor growth in CT26 (87 %) and 4 T1 (82.7 %) tumor-bearing mice, respectively after 19 days	– TBP was organic sonosensitizer that acted ligand – The anchoring of TBP into metal organic layer structure increased ROS production yield by 14.1 times compared to free TBP ligand.	[183]
Zn-TCPP	Zn	tetrakis(4-carboxyphenyl) porphyrin (TCPP)		CT26	Equal dose of TCPP =10 mg/kg	40 kHz	2	30	– Significant antitumor effects not only primary tumors (~100 %) but also secondary tumors (~100 %) (metastasis stimulation)	– Zn improved the ROS generated performance of TCPP, an organic sonosensitizer – Due to high surface area, Zn-TCPP was ideal nano-carrier for cytosine phosphorothioate guanine oligo-deoxynucleotide that allowed synergistic SDT/immunotherapy.	[102]
Al-TCPP	Al	tetrakis(4-carboxyphenyl) porphyrin (TCPP)		4 T1	200 μL(1 mg/mL) each mouse	50 kHz	1.6	6	– Completely suppressed tumor growth after 16 days (estimate ~90 %)	– Al-TCPP performed much higher yield of singlet oxygen and hydroxyl radical under US compared to free TCPP.	[184]
Dy-TCPP	Dy	tetrakis(4-carboxyphenyl) porphyrin (TCPP)		HCT 116	20 μL (400 μg/mL) each mouse	–	1.5	6	– Completely inhibited tumor growth after 21 days (~100 %) (some mice performed tumor eradication after 10 days in Dy-TCPP+US groups)	– Dy-TCPP induced good ROS generation under US. – Dy^{3+} promoted MR imaging as MRI contrast agents. Dy-TCPP could reduce PD-L1 expression that allowed the combinational SDT/immunotherapy	[185]

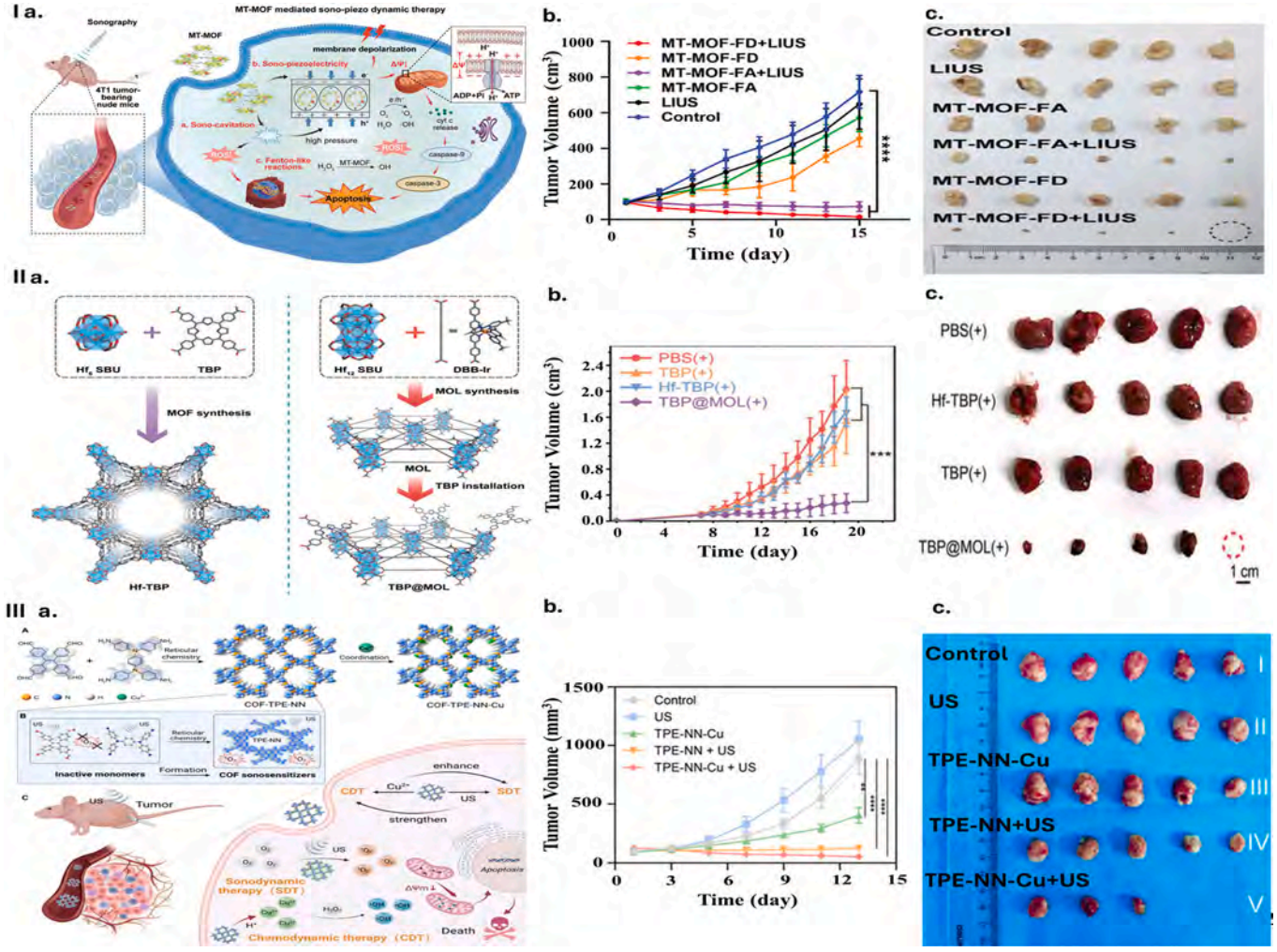

Fig. 7. Schematic illustration of applications of MOFs and COFs in sonodynamic therapy. I. Mn—Ti bimetallic organic framework tetragonal nanosheets (MT-MOF TNS) **a.** The piezoelectric MT-MOF mediated sonodynamic therapy, **b.** Tumor growth curves of mice treated with saline, LIUS, MT-MOF-FA, MT-MOF-FA + LIUS, MT-MOF-FD, and MT-MOF-FD + LIUS (LIUS-low intensity ultrasound), **c.** Photograph of tumors extracted from mice at the end of treatments [180]. **II.** TBP@MOL. **a.** Synthetic procedure of TBP@MOL, **b.** SDT anticancer efficacy in subcutaneous CT26 tumor-bearing BALB/c mice, **c.** Photograph of excised CT26 tumors of BALB/c mice after various treatments [183]. **III.** COF-based sonosensitizer TPE-NN. **a.** Preparation and functionalization of COF sonosensitizers for sono-chemodynamic therapy, **b.** Tumor growth curves of different groups, **c.** Photographs of removed tumors on day 13 of treatments [186]. Copyright 2023, Wiley. Reproduced with permission.

important advantage of these sheets are their biocompatibility and biodegradability [107].

3.4. 2D materials mediated sonothermal therapy (STT)

Unlike SDT, sonothermal therapy is a relatively novel approach that has emerged over the past few years. Due to its novelty, research on this topic is still limited. However, this therapeutic approach is promising and gained significant attention for ongoing studies owing to its great potential in cancer therapy. In this review, we not only summarized fundamental information but also updated recent efforts of STT.

3.4.1. STT mechanism

Unlike conventional STT that relied on incessant formation and explosion of microbubbles to increase the temperature, the STT could also rely on sonothermal agents (STAs) to induce thermal augmentation. Under US irradiation, electrons at stable ground state of STAs are excited and jump to unstable excited singlet state, following by energy release via moving back to stable excited triplet state that is lower energy than singlet state but higher ground state. Recombination of electron and hole pairs also contributes to the energy release. This energy will accumulate and be converted to thermal energy that produces heat during STT process [21]. If the conventional STT requires the high intensity of ultrasound to cause thermal damage, STAs mediated STT allows the utilization of lower intensity ultrasound to protect surrounding normal cells from undesired damages.

3.4.2. 2D sono-thermal agents

Oxygen-vacancy-rich BiO_{2-x} NSs produced piezo-potential ~0.25 V under US illumination that tilted both CB and VB bands to induce piezoelectric effects to generate ROS and ameliorate TME via abating H_2O_2 concentration. Moreover, US also triggered the electron motion that resulted in phonon/lattice thermal vibrations to induce sonothermal effects. The temperature rapidly increased to 65 °C after a short US excitation (96 s). This material allowed the combinational SDT/STT on 4 T1 tumors that exhibited extremely promising antitumor effects after 14 days. The tumors size was not only suppressed but also nearly eliminated [189] (Fig. 8). Edge-hydroxyl graphene nanosheets (EHG) were fabricated with hydroxyl on the edge of sheets to improve their water dispersion. These sheets performed promising sonothermal effects under US irradiation (3 MHz, 1.2 W cm^{-2}) to suppress the growth of 4 T1 tumors. The temperature rapid raised to 47.1 °C under US exposure (2.1

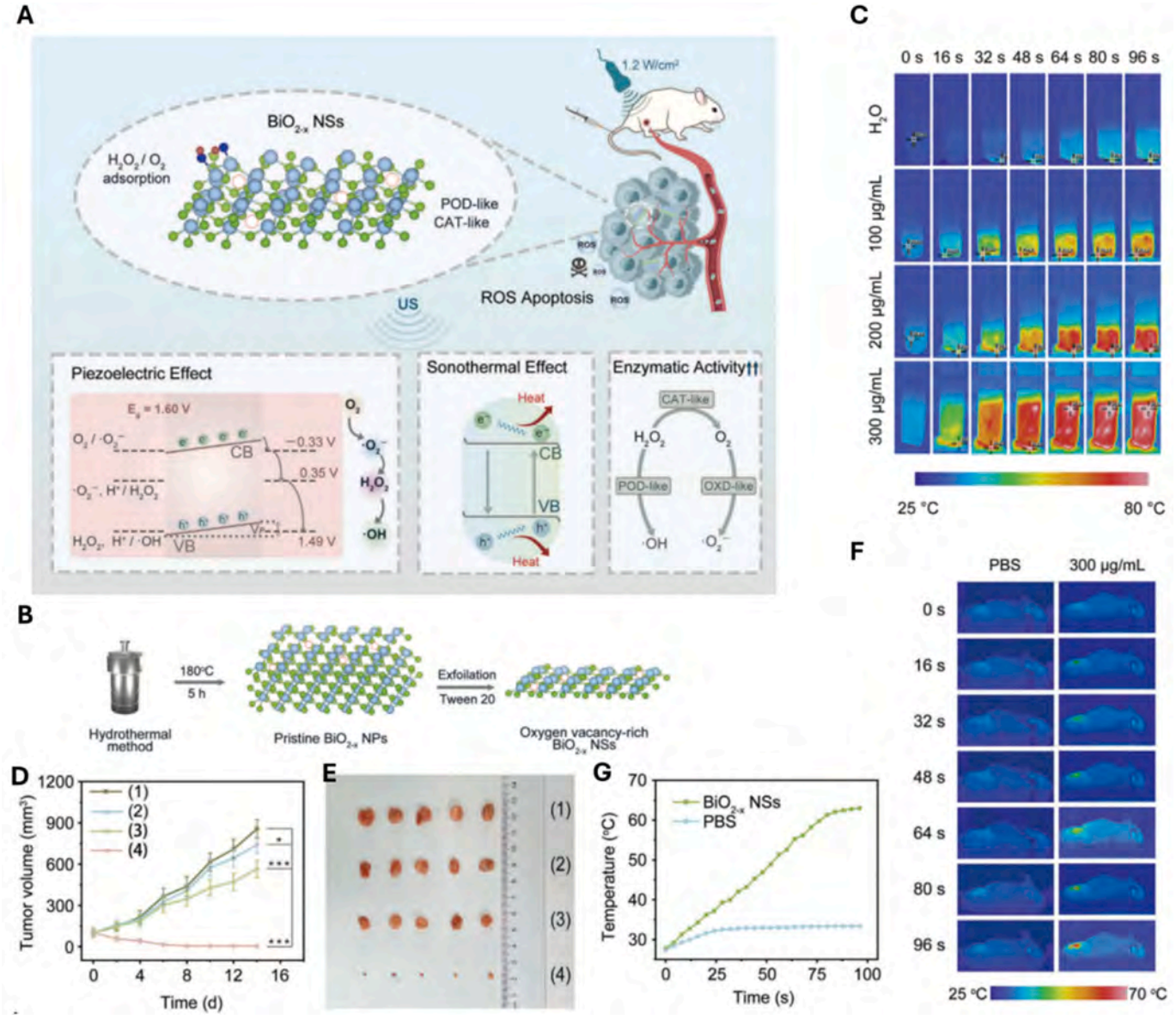

Fig. 8. Oxygen-Vacancy-Rich Piezoelectric BiO_{2-x} Nanosheets for SDT-STT. A. Mechanism of BiO_{2-x} NSs for multimodal treatment of tumors with US assistance, **B.** Synthetic process of BiO_{2-x} NSs, **C.** Infrared thermal imaging of BiO_{2-x} NSs solutions with the concentrations of 100, 200, and 300 μg/mL under US irradiation for different time, **D.** Relative tumor volume growth curves and **E.** Photographs of tumors dissected from 4 T1 tumor-bearing mice treated for 14 days, in which (1) Control, (2) US, (3) BiO_{2-x} NSs, (4) BiO_{2-x} NSs + US, **F.** Corresponding heating profiles and **G.** Infrared thermal imaging of mice treated with PBS group and BiO_{2-x} NSs group after different US times [189]. Copyright 2023, Wiley. Reproduced with permission.

W cm^{-2}). To prolong the time these nanosheets stayed in tumor, nanogel of EHG and poly (N-isopropylacrylamide-*co*-dopamine methacrylamide) was synthesized [190].

3.5. 2D materials supporting sonotherapies

Many 2D materials had vital contributions to synergistic ultrasound-based cancer therapies although they were neither sonosensitizer nor sonothermal agents. Not only providing delivery due to large surface, 2D materials also provided photothermal, chemodynamic or TME amelioration that supported ultrasound-based strategies to overcome barriers to attain better tumoricidal effects.

3.5.1. 2D materials supporting synergistic sonotherapies

Reduced graphene oxide (rGO) nanosheets were used as nanoplatform for modification with TiO_2 for sonodynamic effects and MnO_2 nanoparticles for diagnostic-imaging guidance and monitoring (MnO_x/TiO_2-GR). Moreover, the presence MnO_2 could enhance sonodynamic effects via catalyzing the decomposition of H_2O_2 to O_2 that not only supplied oxygen source for singlet oxygen formation but also alleviated hypoxia and intracellular oxidative stress. rGO contributed to tumoricidal activity with photothermal property. Due to rGO high electroconductivity, the electron-hole pairs separation could be boosted significantly that helped TiO_2 achieving better ROS generation. Under 808 nm laser and US simultaneous irradiation, synergistic photothermal-sonodynamic therapy occurred and eradicated completely 4 T1 tumors in treated mice without reoccurrence after 15 days compared to the tumor inhibition rate of 78 % in only-SDT-treated mice [191].

3.5.2. 2D materials as supporter of sonotherapies

Graphene nanosheets have been used as a bridge for electron transportation between Au and ZnO nanoparticles to trigger ROS generation under US irradiation. The narrow band gap of graphene sheets could

impede the combination of electron -hole pairs to attain higher quantum yield. CT26-tumor bearing mice treated with Au-rGO-ZnO and US exhibited excellent tumor inhibition after 14 days [192].

To overcome the blood-brain barrier (BBB) obstruction in gliomas treatment, YVO4:Nd^{3+}-HMME@MnO_2-LF (YHM) was synthesized for precise theragnostic. A core-shell structure was constructed in which YVO_4:Nd^{3+} particles as the core, MnO_2 nanosheets as the shell and organic sonosensitizer hematoporphyrin monomethyl ether (HMME) anchoring on shell. Lactoferin was modified on the surface for selective ability to cross the BBB. YVO_4:Nd^{3+} acted the role of near-infrared fluorescence imaging and Mn^{2+} acted as MRI contrasting agent for diagnosis. Under US irradiation, MnO_2 nanosheets (shell) were not used as nanocarriers only but also applied as supporter for SDT via GSH depletion and H_2O_2 decomposition to supply O_2 for ROS generation. After 8 days, the C6 tumors in mice treated with YHM and US were successfully inhibited [193].

Liposomes encapsulated sonosensitizer hematoporphyrin monomethyl ether (HMME) and acriflavine (ACF) were coated with MnO_2 nanosheets to form Lipo/HMME/ACF@MnO_2. These particles were modified with AS1411 aptamer via phosphate groups for tumor-targeting drug delivery system. Under US illumination, MnO_2 nanosheets reacted with H_2O_2 to generate O_2 to support HMME-based SDT and reduce intracellular hypoxia. ACF was used as hypoxia-induced factor (HIF-1α/HIF-1β) inhibitor to prevent negative effects after SDT. Beside supporting SDT as mentioned, MnO_2 also caused GSH depletion and acted as MRI contrasting agent. These pH/glutathione/ultrasound-triple responsive nanoparticles exhibited obvious tumoricidal effects on SKOV-3 tumors after 12 days of SDT treatment [194].

4. Advantages and limitations

Take together, it has been shown that that sonotherapies and their combinational modalities provided inevitably excellent antitumor outcomes. In some specific cases, tumors were utterly eradicated in short treatment periods. Besides effective tumoricidal effects, there are still many challenges that need to be addressed prior to clinical translation.

4.1. Using ultrasound

4.1.1. Advantages

Ultrasound, owing to its deep tissue penetration capabilities, presents a promising alternative to conventional light-based therapies in cancer treatment. This modality offers a novel avenue for addressing tumor types that are challenging to treat due to their deep anatomical location and extensive vascular networks. Moreover, US serves as an external and controllable irradiation source, enabling a non-invasive and localized therapeutic approach that specifically targets the tumor area. This minimizes the potential for collateral damage to surrounding tissues and mitigates the long-term adverse effects typically associated with traditional treatment modalities, such as surgery, chemotherapy, or radiotherapy.

Sonotherapies harness the generation of reactive oxygen species (ROS) or heat under ultrasound irradiation to induce lethal effects on primary tumors and contribute positively to inhibiting metastasis. Additionally, US-activated processes can induce DNA damages in tumor cells, reduce expression of metastatic factors such as hypoxia inducible or angiogenic ones, while simultaneously triggering immune responses. These mechanisms enable US-based strategies to hinder the metabolic adaptations that render tumors resistant to conventional therapeutic interventions. Therefore, sonotherapies are promising tools for resistant cancer cells treatment such 4 T1, etc.

Due to high tumoricidal effects, US-activated therapeutic modalities allow shorter treatment periods (usually less than 15 days) with significant tumor growth inhibition.

4.1.2. Limitations

Despite advancements in penetration ability, US-based treatments still face limitations compared to phototherapies. Firstly, the hypoxic conditions in tumors negatively affect sonodynamic performance, especially Type II sonodynamic therapy (SDT), which is related to the generation of singlet oxygen ($^1O_2$) from ambient O_2. Secondly, the heat produced during sonothermal therapy (STT) could trigger the development of heat shock proteins, which may prevent the complete destruction of cancer cells if the heat is not sufficient. Moreover, the shear force and thermal effects caused by cavitation when high-intensity ultrasound is used could lead to undesired physical damage to healthy cells. Therefore, selectivity, particularly high-targeting delivery, is critically required.

Studies on ultrasound-activated therapeutic modalities are still limited compared to phototherapies due to their novelty. The mechanisms behind both sonodynamic and sonothermal effects remain under debate, with many tentative explanations. Better understanding of precise mechanisms will enable further research and development.

Despite their inherent anticancer potential, monotherapy strategies based solely on SDT or STT typically suppress cancer cell proliferation and reduce tumor size rather than completely eradicating the tumor. Combining these therapies with other therapeutic modalities is necessary for full tumor removal. Moreover, most studies on sonotherapies are still in infancy and their preclinical or clinical applications are still unexplored areas.

4.2. Using 2D materials to overcome limitations of sonotherapies

4.2.1. Benefits

Firstly, two-dimensional materials possess large surface areas adorned with numerous functional groups at their edges and on their surfaces. This unique characteristic facilitates surface engineering through modification with a variety of active compounds, including drugs, gas donors, polymers, and targeting molecules. Such modifications not only enhance the physicochemical properties of these materials but also improve their ability to deliver therapeutic agents. For instance, drugs or gas donors' modifications enable the synergistic effects of combination therapies such as chemo-sonotherapy and sono-gas therapy, significantly amplifying tumoricidal effects. Modifications with polymers or ligands improve biocompatibility, bioavailability, and aqueous dispersion, which help reduce clearance by the reticuloendothelial system (RES), extend blood circulation time, and increase tumor accumulation of 2D sonosensitizers or sonothermal agents. Additionally, the attachment of targeting molecules facilitates active recognition and precise targeting of cancerous tissues, thus enhancing therapeutic outcomes by selectively attacking tumors and minimizing damage to surrounding healthy tissues.

Secondly, 2D materials play a pivotal role in mediating combinational ultrasound-based therapies, thereby enhancing synergistic effects. Some 2D materials exhibit intrinsic photothermal, photodynamic, and chemodynamic properties in addition to their US-induced capabilities, enabling multi-modal treatment strategies such as PTT/SDT, PDT/STT, and CDT/SDT. These combined approaches significantly improve therapeutic efficacy, particularly in achieving complete tumor eradication rather than merely suppressing tumor growth. Furthermore, the integration of multiple therapeutic mechanisms not only prevents the development of treatment-resistant tumors but also overcomes the limitations associated with monotherapy. Consequently, synergistic multi-therapy strategies can reduce treatment duration and accelerate patient recovery.

Lastly, doping 2D materials with single atoms offers significant enhancement in both sonodynamic and sonothermal performance, while providing additional therapeutic benefits. Specific metal atoms, such as Mn, Fe, and Cu, etc. can catalyze Fenton reactions to induce chemodynamic effects, mitigate tumor microenvironment via GSH depletion, and enhance bioimaging by improving MRI contrast. The incorporation

of Pt, Au, or Mn, etc. allows the decomposition of H_2O_2 to O_2 that not only ameliorates hypoxic conditions to prevent the expression of metastatic factors (HIF1) but also supplies oxygen source to overcome the limitations of SDT, especially SDT type II that depends on transformation of ambient O_2 to produce singlet oxygen.

4.2.2. Challenges

Despite several breakthroughs in employing 2D materials as sono-activable agents, several significant challenges must be addressed before these materials can be widely adopted for sonotherapy in preclinical or clinical trials.

Firstly, synthesis of 2D sono-activatable agents requires a complex and costly process. Despite excellent antitumor performance under ultrasound, their fabrication and modification present substantial difficulties in scaling up due to utilization of complex equipment, specific condition and careful handling. Even minor errors in the scaling-up process can result in significant changes to the materials' structure and properties that compromise therapeutic effects in cancer treatments. This challenge remains a key issue requiring further investigation.

Secondly, biosafety and potential side effects are critical concerns besides the good therapeutic performance. Although ultra-thinness and surface engineering could improve biocompatibility, long blood circulation and tumor recognition abilities, the safety and long-term effects of 2D materials remain underexplored. The existing studies primarily focus on the in vitro cytotoxicity and in vivo mice experiments to evaluate their biocompatibility; however, there is a lack of research on the degradation pathways or the long-term toxicity of these materials. The extended circulation time in the bloodstream, while beneficial for treatment, raises concerns regarding the potential impact on human metabolism and the possibility of unwanted side effects, especially 2D sono-activatable agents utilizing non- dietary elements such as bismuth, tungstane, irradium and niobium, etc.

Thirdly, there is considerable variability in ultrasound parameters across studies examining sonotherapies, including differences in intensity, treatment duration, and frequency. This inconsistency poses a significant barrier to comparing therapeutic effectiveness and translating the technology into preclinical and clinical applications. Additionally, it is challenging for a single US machine to accommodate multiple different US frequencies. In preclinical and clinical applications, using multiple pieces of equipment to generate different US irradiations for only a few materials is both time-consuming and costly. Therefore, standardizing ultrasound parameters across studies would not only facilitate more accurate therapeutic evaluations but also reduce costs and streamline the transition to clinical practice. Moreover, differences in dosage and modification approaches present major barriers to comparing treatment outcomes between the main material groups, making it difficult to determine which materials are most suitable for further clinical investigation. Additionally, the variations in ROS detection methods, in vitro and in vivo evaluations, as well as the frequency and regimen of treatments, are major challenges in comparing therapeutic efficacy across studies. For instance, it is difficult to compare outcomes between one study in which mice receive US treatment 3 times over 15 days and another in which mice are treated with US 5 to 7 times over 16 days. The number of US irradiation and the overall treatment duration can significantly influence therapeutic outcomes.

Finally, the transition from animal models to clinical trials represents a major challenge. The substantial differences between mice and humans in terms of body size, metabolic pathways, and life expectancy are the main obstacles to clinical translation. In mice models, tumors are typically generated on the flanks, meaning they are located close to the body surface and covered only by thin tissue layers. Nanomedicines are commonly administered via intravenous injection through the tail vein, and the distance between this vein and the tumor site is relatively short. As a result, ultrasound can easily penetrate and reach the tumor without significant energy loss through heat conversion caused by absorption in soft tissues. Nanodrugs delivery to tumors in animal experiments often demonstrate high targeting efficiency and good accumulation. In contrast, humans are approximately 2500 times larger than mice (with an average body weight of ~70 kg compared to 20–27 g for a mouse). The human cardiovascular system is also more complex. Tumors in humans are usually located in internal organs such as the liver, kidneys, or lungs, where they are situated deep inside the body, covered by thick tissue layers, and surrounded by dense blood vessels, unlike the superficial flank tumors of mice. Therefore, ultrasound energy may diminish substantially when traveling through human tissues, potentially reducing the therapeutic efficacy observed in animal models. Moreover, nanomedicine delivery in humans often fails to achieve the same efficient tumor distribution observed in mice. Metabolic pathways in mice differ considerably from those in humans. Certain metabolic mechanisms in humans do not occur in mice, and vice versa. Therefore, the human body may respond to nanomedicines in ways that differ significantly from animal works. Additionally, in vivo studies using small animals such as mice, rats, and rodents usually occur in limited durations (less than 60 days) due to their short life spans, while human life extends over decades. This raises unresolved concerns about long-term biodegradation, off-target accumulation, and potential toxicity of nanomedicines in the human body, particularly for 2D nanomaterials derived from heavy metals or non-dietary elements [195,196].

5. Conclusions

In this review, we comprehensively discuss the crucial roles of 2D materials in US-based cancer therapies, including their functions as nanocarriers, sono-activatable agents (sonosensitizers and sonothermal agents), and supportive components for sonotherapies and their combinational modalities. A concise yet comprehensive summary of recent research advancements in the diverse applications of 2D materials in sonotherapies (sonodynamic and sonothermal) is meticulously presented. Fundamental aspects, including underlying mechanisms and strategies to enhance therapeutic effects, are thoroughly discussed. Additionally, the advantages and limitations of these materials are examined through their classification into major groups, such as carbon and its derivatives, carbon nitrides, black phosphorus, MXenes, and layered double hydroxides.

In sonodynamic therapy, 2D materials have been widely applied as sonosensitizers due to their piezoelectric effects under US, which trigger reactive oxygen species (ROS) production to induce apoptosis. Their large surface area and functional groups at the edges enable modifications that not only enhance therapeutic performance through combination with other strategies but also significantly improve their physicochemical properties and tumor recognition abilities for precise targeted delivery.

There are three key approaches to enhancing sonodynamic performance by amplifying piezoelectric effects: defect introduction, single-atom doping, and heterojunction construction. These strategies improve treatment outcomes by enhancing sonodynamic efficiency and enabling synergistic theranostic applications using multifunctional 2D nanosheets. Promising therapeutic results, including complete tumor eradication, have been achieved through SDT-based combination therapies utilizing 2D materials, whereas US-based monotherapy typically leads to tumor growth inhibition.

Sonothermal therapy is still in the early stages of development, with a limited number of studies available. However, its reported exceptional tumoricidal effects highlight its potential as a promising candidate for cancer treatment.Although overcoming the limitation of deep tissue penetration is crucial, several challenges remain, including biosafety, biodegradation, scalability, mechanism elucidation, and standardization of ultrasound parameters. These must be addressed before successful preclinical and clinical translation of sonotherapies can be achieved. Nevertheless, the promising antitumor effects of sonotherapies position them as a potential breakthrough in cancer treatment, despite being in their early stages and requiring further exploration.

Declaration of competing interest

The authors declare the following financial interests/personal relationships which may be considered as potential competing interests: Hang Thu Ta reports financial support was provided by Australian Research Council. If there are other authors, they declare that they have no known competing financial interests or personal relationships that could have appeared to influence the work reported in this paper.

Acknowledgement

NAT is supported by a PhD scholarship from Griffith University. HTT is supported by an ARC Future Fellowship (FT240100280).

Data availability

No data was used for the research described in the article.

References

[1] K.X. Vazquez-Prada, S.S. Moonshi, Z.P. Xu, H.T. Ta, Appl. Mater. Today 35 (2023).
[2] S.S. Moonshi, K.X. Vazquez-Prada, H. Adelnia, N.J.W. van Holthe, Y. Wu, J. Tang, A.C. Bulmer, H.T. Ta, Appl. Mater. Today 37 (2024) 102150.
[3] S.S. Moonshi, K.X. Vazquez-Prada, J. Tang, N.J. Westra van Holthe, G. Cowin, Y. Wu, H.D. Tran, R. Mckinnon, A.C. Bulmer, H.T. Ta, ACS Appl. Mater. Interfaces 15 (2023) 42153–42169.
[4] N. Anh Tran, M. Seok Song, G. Kim, N. Binh Nguyen, N. Hoàng Ly, S.Y. Lee, S.-W. Joo, Appl. Surf. Sci. 604 (2022).
[5] J. Roy, V. Pandey, I. Gupta, H. Shekhar, ACS Biomater. Sci. Eng. 7 (2021) 5326–5338.
[6] X. Lin, S. Chen, Y. Su, Y. Wu, L. Huang, Q. Ye, J. Song, Adv. Sci. (Weinh) 11 (2024) e2306301.
[7] P. Chen, P. Zhang, N.H. Shah, Y. Cui, Y. Wang, Int. J. Mol. Sci. 24 (2023).
[8] Y. Qi, S. Ren, J. Ye, S. Bi, L. Shi, Y. Fang, G. Wang, Y.Z. Finfrock, J. Li, Y. Che, G. Ning, Adv. Healthc. Mater. 12 (2023) e2300291.
[9] J. Li, Z. Yue, M. Tang, W. Wang, Y. Sun, T. Sun, C. Chen, Adv. Healthc. Mater. 13 (2024) e2302028.
[10] Z. Ma, M. Yuan, Z. Cheng, Z. Yang, L. Yang, B. Liu, Y. Bian, A.A. Al Kheraif, P. A. Ma, J. Lin, Chem. Eng. J. 482 (2024).
[11] R. Jin, G. Zhang, L. Tang, M. Li, M. Yang, J. Li, Z. Wang, F. Guan, ACS Appl. Nano Mater. 7 (2024) 3968–3976.
[12] F. Yang, J. Dong, Z. Li, Z. Wang, ACS Nano 17 (2023) 4102–4133.
[13] Y. Opoku-Damoah, Z.P. Xu, H.T. Ta, R. Zhang, ACS Appl. Bio Mater. 7 (2024) 7585–7594.
[14] C. Wang, R. Zhang, J. He, L. Yu, X. Li, J. Zhang, S. Li, C. Zhang, J.C. Kagan, J. M. Karp, R. Kuai, Nat. Commun. 14 (2023) 3877.
[15] H. Lei, J.H. Kim, S. Son, L. Chen, Z. Pei, Y. Yang, Z. Liu, L. Cheng, J.S. Kim, ACS Nano 16 (2022) 10979–10993.
[16] Y. Li, W. Chen, Y. Kang, X. Zhen, Z. Zhou, C. Liu, S. Chen, X. Huang, H.J. Liu, S. Koo, N. Kong, X. Ji, T. Xie, W. Tao, Nat. Commun. 14 (2023) 6973.
[17] J. Ouyang, S. Rao, R. Liu, L. Wang, W. Chen, W. Tao, N. Kong, Adv. Drug Deliv. Rev. 185 (2022) 114268.
[18] L. Zhao, J. Ji, N. Wang, C. Kong, Y. Yang, X. Lu, B. Geng, S. Qin, X. Feng, Z. Cao, Chem. Eng. J. 500 (2024).
[19] G. Li, H. Lei, Y. Yang, X. Zhong, F. Gong, Y. Gong, Y. Zhou, Y. Zhang, H. Shi, Z. Xiao, Z. Dong, L. Cheng, Adv. Sci. (Weinh) 9 (2022) e2201069.
[20] M. Zhang, D. Sun, H. Huang, D. Yang, X. Song, W. Feng, X. Jing, Y. Chen, Adv. Mater. 36 (2024) e2409663.
[21] F. Hakimi, Z. Ma, N. Karimi, F. Sefat, Z. Cheng, J. Lin, A. Maleki, Adv. Funct. Mater. 35 (2024) 2420859.
[22] H. Huang, Y. Miao, Y. Li, Coord. Chem. Rev. 523 (2025).
[23] J.F. Diaz-Alejo, I. Gonzalez Gomez, J. Earl, Oncol. Rev. 16 (2022) 531.
[24] X. Liu, X. Pan, C. Wang, H. Liu, Particuology 75 (2023) 199–216.
[25] T. Zhang, Y. Sun, J. Cao, J. Luo, J. Wang, Z. Jiang, P. Huang, J. Nanobiotechnol. 19 (2021) 315.
[26] P. Datta, S. Moolayadukkam, D. Chowdhury, A. Rayes, N.S. Lee, R.P. Sahu, Q. Zhou, I.K. Puri, BME Front. 2024 (2024) 0080.
[27] H. Ding, H. Yu, Y. Dong, R. Tian, G. Huang, D.A. Boothman, B.D. Sumer, J. Gao, J. Control. Release 156 (2011) 276–280.
[28] N. Frazier, A. Payne, J. de Bever, C. Dillon, A. Panda, N. Subrahmanyam, H. Ghandehari, J. Control. Release 241 (2016) 186–193.
[29] L. Zhu, M.B. Altman, A. Laszlo, W. Straube, I. Zoberi, D.E. Hallahan, H. Chen, Ultrasound Med. Biol. 45 (2019) 1025–1043.
[30] Y.S. Kim, H. Rhim, M.J. Choi, H.K. Lim, D. Choi, Korean J. Radiol. 9 (2008) 291–302.
[31] T. Entradas, S. Waldron, M. Volk, J. Photochem. Photobiol. B 204 (2020) 111787.
[32] M. He, X. Wang, H. Yu, Y. Zhao, L. Zhang, Z. Xu, Y. Kang, P. Xue, Biomaterials 305 (2024) 122446.
[33] Z. Yang, M. Yuan, B. Liu, Z. Ma, J. Ma, X. Ma, K. Li, P. Ma, Z. Cheng, J. Lin, Adv. Mater. 37 (2025) e2412069.
[34] Z. Shi, Y. Zeng, J. Luo, X. Wang, G. Ma, T. Zhang, P. Huang, ACS Nano 18 (2024) 28659–28674.
[35] Q. Duan, H. Li, J. Xue, Q. Zhang, J. Gao, X. Wang, Q. Zhang, X. Guo, L. Guo, P. Li, X. Wang, S. Sang, Y. Xi, Mol. Pharm. 21 (2024) 760–769.
[36] C. You, X. Li, D. Wang, H. Chen, L. Liang, Y. Chen, Y. Zhao, H. Xiang, Angew. Chem. Int. Ed. Eng. 61 (2022) e202210174.
[37] J. Wang, J. Huang, W. Zhou, J. Zhao, Q. Peng, L. Zhang, Z. Wang, P. Li, R. Li, J. Nanobiotechnol. 19 (2021) 87.
[38] X. Lin, T. He, R. Tang, Q. Li, N. Wu, Y. Zhou, H. He, L. Wan, J. Huang, Q. Jiang, Y. Zhong, Z. Xie, Z. Hu, Y. Zhou, P. Li, J. Nanobiotechnol. 20 (2022) 80.
[39] P. Wang, L. Ren, Y. Tang, B. Yuan, B. Geng, Y. Zhao, Chem. Eng. J. 500 (2024).
[40] E.T.P. Ayala, I.S.E. Carvalho, C.A. Antunes, A. Mahmood, M.B. Requena, F. Alves, L. Pires, V. Yakovlev, V.S. Bagnato, S. Pratavieira, Sci. Rep. 15 (2025) 30859.
[41] H. Wang, D. Li, H. Wang, Q. Ren, Y. Pan, A. Dao, D. Wang, Z. Wang, P. Zhang, H. Huang, J. Med. Chem. 67 (2024) 18356–18367.
[42] H. Tsukihara, F. Nakagawa, K. Sakamoto, K. Ishida, N. Tanaka, H. Okabe, J. Uchida, K. Matsuo, T. Takechi, Oncol. Rep. 33 (2015) 2135–2142.
[43] J.G. Xu, S. Chen, Y. He, X. Zhu, Y. Wang, Z. Ye, J.C. Zhou, X. Wu, L. Zhang, X. Ren, H. Jia, H. Yu, X. Wei, Y. Feng, X. Chen, X. Cui, X. Pan, S. Wang, S. Xia, H. Shang, Y. Pu, W. Xu, H. Li, Q. Chen, Z. Chen, M. Wang, X. Yan, H. Shi, M. Li, Y. Xia, R. Bellelli, S. Dong, J. He, J. Huang, C.L. Cai, X. Zhu, Y. Zhan, L. Wan, Nat. Commun. 15 (2024) 10872.
[44] N.A. Tran, S.S. Moonshi, A.K. Lam, C.T. Lu, C.Q. Vu, S. Arai, H.T. Ta, Cancer Metastasis Rev. 44 (2025) 51.
[45] C. Liao, X. Liu, C. Zhang, Q. Zhang, Semin. Cancer Biol. 88 (2023) 172–186.
[46] B. Muz, P. de la Puente, F. Azab, A.K. Azab, Hypoxia (Auckl) 3 (2015) 83–92.
[47] N.A. Baird, D.W. Turnbull, E.A. Johnson, J. Biol. Chem. 281 (2006) 38675–38681.
[48] K. Musaie, S. Abbaszadeh, K. Marais, V. Nosrati-Siahmazgi, S. Rezaei, B. Xiao, K. Dua, H.A. Santos, M.A. Shahbazi, Adv. Funct. Mater. 35 (2025).
[49] F.J. Lei, J.Y. Chiang, H.J. Chang, D.C. Chen, H.L. Wang, H.A. Yang, K.Y. Wei, Y. C. Huang, C.C. Wang, S.T. Wei, C.H. Hsieh, Redox Biol. 65 (2023) 102831.
[50] Y. Tie, F. Tang, Y.Q. Wei, X.W. Wei, J. Hematol. Oncol. 15 (2022) 61.
[51] A. Zhang, X. Zheng, G. Yan, X. Liu, D. Xie, X. Xu, M. Sun, Z. Liu, J. Nanobiotechnol. 23 (2025) 548.
[52] M. Pan, D. Hu, L. Yuan, Y. Yu, Y. Li, Z. Qian, Acta Pharm. Sin. B 13 (2023) 2926–2954.
[53] E. Desideri, F. Ciccarone, M.R. Ciriolo, Nutrients 11 (2019).
[54] G. Cheng, S. Tao, S. Liu, P. Wang, C. Zhang, J. Liu, C. Hao, S. Wang, D. Guo, B. Xu, ACS Macro Lett. 13 (2024) 599–606.
[55] N. Roy, P. Paira, ACS Omega 9 (2024) 20670–20701.
[56] Y. Tian, P. Li, L. Wang, X. Ye, Z. Qu, J. Mou, S. Yang, H. Wu, Biomater. Sci. 12 (2024) 2341–2355.
[57] D. Ma, Y. Wang, A. Liu, S. Li, C. Lu, C. Chen, Catalysts 8 (2018).
[58] S. Sachdeva, A. Pustovarenko, E.J.R. Sudhölter, F. Kapteijn, L.C.P.M. de Smet, J. Gascon, CrystEngComm 18 (2016) 4018–4022.
[59] H. Zeng, X. Cui, Chem. Soc. Rev. 44 (2015) 2629–2642.
[60] R.M. Ronchi, J.T. Arantes, S.F. Santos, Ceram. Int. 45 (2019) 18167–18188.
[61] A.-E. Stamate, O.D. Pavel, R. Zavoianu, I.-C. Marcu, Catalysts 10 (2020).
[62] V.V. Kulish, O.I. Malyi, C. Persson, P. Wu, Phys. Chem. Chem. Phys. 17 (2015) 992–1000.
[63] A. Jayakumar, S. Mathew, S. Radoor, J.T. Kim, J.-W. Rhim, S. Siengchin, Mater. Today Chem. 30 (2023).
[64] N. Baig, Compos. A: Appl. Sci. Manuf. 165 (2023).
[65] A. Bolotsky, D. Butler, C. Dong, K. Gerace, N.R. Glavin, C. Muratore, J. A. Robinson, A. Ebrahimi, ACS Nano 13 (2019) 9781–9810.
[66] A. Murali, G. Lokhande, K.A. Deo, A. Brokesh, A.K. Gaharwar, Mater. Today (Kidlington) 50 (2021) 276–302.
[67] M.J. Molaei, J. Drug Deliv. Sci. Technol. 61 (2021).
[68] B. Ma, A. Bianco, Small 17 (2021) e2102557.
[69] T. Tong, H. Lei, S. Zhang, D. Jiang, Y. Guan, C. Xing, H. Chen, X. Yang, Y. Kang, J. Pang, Adv. Healthc. Mater. 11 (2022) e2201472.
[70] M. Du, T. Wang, W. Peng, R. Feng, M. Goh, Z. Chen, J. Nanobiotechnol. 22 (2024) 167.
[71] R. Davis Jr., R.A. Urbanowski Jr., A.K. Gaharwar, Curr. Opin Biomed. Eng. 20 (2021).
[72] Y. Zheng, Y. Liu, F. Wei, H. Xiao, J. Mou, H. Wu, S. Yang, Acta Biomater. 121 (2021) 592–604.
[73] Y.W. Chen, T.Y. Liu, P.H. Chang, P.H. Hsu, H.L. Liu, H.C. Lin, S.Y. Chen, Nanoscale 8 (2016) 12648–12657.
[74] X. Zhou, S. Wu, X. Wang, Z. Wang, Q. Zhu, J. Sun, P. Huang, X. Wang, W. Huang, Q. Lu, Front. Mech. Eng. 19 (2024).
[75] M. Zhu, Q. Liu, W.Y. Wong, L. Xu, Adv. Mater. (2025) 2419970.
[76] S. Bairagi, I. Shahidul, M. Shahadat, D.M. Mulvihill, W. Ali, Nano Energy 111 (2023).
[77] M. Zhu, Z. Yi, B. Yang, C. Lee, Nano Today 36 (2021).
[78] F. Yang, P. Wang, J. Hao, J. Qu, Y. Cai, X. Yang, C.M. Li, J. Hu, Nano Energy 118 (2023).
[79] X. Zhou, B. Shen, A. Lyubartsev, J. Zhai, N. Hedin, Nano Energy 96 (2022).
[80] Y.T. Wang, H.Y. Lin, Y.C. Chen, Y.G. Lin, J.M. Wu, Small Methods 8 (2024) e2301287.
[81] D. Liu, A. Barbar, T. Najam, M.S. Javed, J. Shen, P. Tsiakaras, X. Cai, Appl. Catal. B Environ. 297 (2021).

[82] B. Tian, R. Tian, S. Liu, Y. Wang, S. Gai, Y. Xie, D. Yang, F. He, P. Yang, J. Lin, Adv. Mater. 35 (2023) e2304262.
[83] Q. Wu, J. Zhang, X. Pan, Z. Huang, H. Zhang, J. Guo, Y. Xue, R. Shi, H. Liu, Adv. Sci. (Weinh) 10 (2023) e2301152.
[84] Y. Dong, S. Dong, B. Liu, C. Yu, J. Liu, D. Yang, P. Yang, J. Lin, Adv. Mater. 33 (2021) e2106838.
[85] J. Gupta, P.A. Hassan, K.C. Barick, Defects in Nanomaterials for Visible Light Photocatalysis, in: Nanostructured Materials for Visible Light Photocatalysis, 2022, pp. 319–350.
[86] D.-M. Liu, J.-T. Zhang, C.-C. Jin, B.-B. Chen, J. Hu, R. Zhu, F. Wang, Nano Energy 95 (2022).
[87] J. Yang, H. Song, Y. Zhang, X. Zhu, Surf Interfaces 24 (2021).
[88] L. Wang, J. Yu, Principles of photocatalysis, in: S-scheme Heterojunction Photocatalysts - Fundamentals and Applications, 2023, pp. 1–52.
[89] J. Low, J. Yu, C. Jiang, Design and Fabrication of Direct Z-Scheme Photocatalysts, in: Surface Science of Photocatalysis, 2020, pp. 193–229.
[90] G. Feng, H. Huang, M. Zhang, Z. Wu, D. Sun, Q. Chen, D. Yang, Y. Zheng, Y. Chen, X. Jing, Adv. Sci. (Weinh) 10 (2023) e2302579.
[91] C. Yu, Y. Dong, X. Zhu, L. Feng, P. Zang, B. Liu, S. Dong, R. Zhao, R. Xu, P. Yang, Nano Lett. 24 (2024) 8008–8016.
[92] E. Falcone, A.G. Ritacca, S. Hager, H. Schueffl, B. Vileno, Y. El Khoury, P. Hellwig, C.R. Kowol, P. Heffeter, E. Sicilia, P. Faller, J. Am. Chem. Soc. 144 (2022) 14758–14768.
[93] W. Zhang, J. Gao, L. Lu, T. Bold, X. Li, S. Wang, Z. Chang, J. Chen, X. Kong, Y. Zheng, M. Zhang, J. Tang, NanoImpact 23 (2021) 100338.
[94] Z. Yang, M. Yuan, Z. Cheng, B. Liu, Z. Ma, J. Ma, J. Zhang, X. Ma, P. Ma, J. Lin, Angew. Chem. Int. Ed. Eng. 63 (2024) e202401758.
[95] S. Yang, T. Hu, G.R. Williams, Y. Yang, S. Zhang, J. Shen, M. Chen, R. Liang, L. Lyu, J. Nanobiotechnol. 22 (2024) 317.
[96] L. Cheng, S. Qiu, J. Wang, W. Chen, J. Wang, W. Du, L. Song, Y. Hu, Colloids Surf. A Physicochem. Eng. Asp. 638 (2022).
[97] B. Geng, J. Hu, X. He, Z. Zhang, J. Cai, D. Pan, L. Shen, Adv. Mater. 36 (2024) e2313670.
[98] L. Huang, S. Zhao, J. Wu, L. Yu, N. Singh, K. Yang, M. Lan, P. Wang, J.S. Kim, Coord. Chem. Rev. 438 (2021).
[99] M. Overchuk, R.A. Weersink, B.C. Wilson, G. Zheng, ACS Nano 17 (2023) 7979–8003.
[100] C. Kong, X. Chen, Int. J. Nanomedicine 17 (2022) 6427–6446.
[101] D. Zhu, Y. Lu, S. Yang, T. Hu, C. Tan, R. Liang, Y. Wang, Adv. Sci. (Weinh) 11 (2024) e2401064.
[102] W. Zhu, Q. Chen, Q. Jin, Y. Chao, L. Sun, X. Han, J. Xu, L. Tian, J. Zhang, T. Liu, Z. Liu, Nano Res 14 (2020) 212–221.
[103] S. Cheng, T. Zhou, Y. Luo, J. Zhang, K. Dong, Q. Zhang, W. Shu, T. Zhang, Q. Zhang, R. Shi, Y. Yao, H. Wang, J. Nanobiotechnol. 22 (2024) 408.
[104] L. Sun, W. Gao, J. Wang, X. Niu, N. Kurniawan, L. Li, Z.P. Xu, Small 19 (2022).
[105] Y. Wu, Z. Zhao, M. Ma, W. Zhang, W. Liu, X. Liang, T. Zhao, Y. Luo, Y. Wang, M. Li, T. Li, C. Liu, X. Luo, S. Wang, W. Li, W. Zeng, H. Wang, W. Li, T. Wu, Z. Ke, F. Luo, Theranostics 15 (2025) 1456–1477.
[106] S. Liang, J. Yao, D. Liu, L. Rao, X. Chen, Z. Wang, Adv. Mater. 35 (2023) e2211130.
[107] W. Dai, H. Dong, X. Zhang, ACS Appl. Mater. Interfaces 16 (2024) 56696–56704.
[108] Z. Yang, Z. Li, C. Yang, L. Meng, W. Guo, L. Jing, Adv. Sci. (Weinh) 12 (2025) e2410621.
[109] Y.Y. Ju, X.X. Shi, S.Y. Xu, X.H. Ma, R.J. Wei, H. Hou, C.C. Chu, D. Sun, G. Liu, Y. Z. Tan, Adv. Sci. (Weinh) 9 (2022) e2105034.
[110] B. Geng, J. Hu, Y. Li, S. Feng, D. Pan, L. Feng, L. Shen, Nat. Commun. 13 (2022) 5735.
[111] A. Thomas, A. Fischer, F. Goettmann, M. Antonietti, J.-O. Müller, R. Schlögl, J. M. Carlsson, J. Mater. Chem. 18 (2008).
[112] M. Chen, Y. Zhang, L. Cui, Z. Cao, Y. Wang, W. Zhang, Y. Zheng, D. Sun, L. Zheng, S. Kang, D. Zhang, Chem. Eng. J. 422 (2021).
[113] W. Ma, J. Lu, B. Wan, D. Peng, Q. Xu, G. Hu, Y. Peng, C. Pan, Z.L. Wang, Adv. Mater. 32 (2020) e1905795.
[114] Z. Li, T. Zhang, F. Fan, F. Gao, H. Ji, L. Yang, J. Phys. Chem. Lett. 11 (2020) 1228–1238.
[115] W. Du, W. Chen, J. Wang, L. Cheng, J. Wang, H. Zhang, L. Song, Y. Hu, X. Ma, Biomater. Adv. 136 (2022) 212794.
[116] X. Zhu, S. Zhang, Y. Cao, X. Ge, Y. Huang, F. Mao, B. Chen, J. Li, Y. Xu, A. Wu, Chin. Chem. Lett. 34 (2023).
[117] Y. Zhu, G. Arkin, T. He, F. Guo, L. Zhang, Y. Wu, P.N. Prasad, Z. Xie, Int. J. Pharm. 655 (2024) 124015.
[118] T. Chen, W. Zeng, C. Tie, M. Yu, H. Hao, Y. Deng, Q. Li, H. Zheng, M. Wu, L. Mei, Bioact Mater 10 (2022) 515–525.
[119] S. Wu, G. Li, W. Ouyang, Y. Tian, S. Li, W. Wu, H. Liu, Biomater. Res. 28 (2024) 0014.
[120] A.A. Altalhi, E.A. Mohamed, N.A. Negm, Energy Adv. 3 (2024) 2136–2151.
[121] Q. Xu, X. Gao, S. Zhao, Y.N. Liu, D. Zhang, K. Zhou, H. Khanbareh, W. Chen, Y. Zhang, C. Bowen, Adv. Mater. 33 (2021) e2008452.
[122] L. Li, I. Soyhan, E. Warszawik, P. van Rijn, Adv. Sci. (Weinh) 11 (2024) e2306035.
[123] G. Li, Y. Guo, C. Ni, Z. Wang, M. Zhan, H. Sun, G. Choi, J.H. Choy, X. Shi, M. Shen, J. Mater. Chem. B 12 (2024) 7429–7439.
[124] L. Yan, S. Gonca, G. Zhu, W. Zhang, X. Chen, J. Mater. Chem. B 7 (2019) 5583–5601.
[125] W. Tang, J. Wu, L. Wang, K. Wei, Z. Pei, F. Gong, L. Chen, Z. Han, Y. Yang, Y. Dai, X. Cui, L. Cheng, ACS Nano 18 (2024) 10495–10508.
[126] M. Cao, S. Yang, J. Li, Y. Yang, L. Zhan, T. Wang, T. Hu, R. Liang, Z. Li, Small 20 (2024) e2404475.
[127] T. Hu, W. Shen, F. Meng, S. Yang, S. Yu, H. Li, Q. Zhang, L. Gu, C. Tan, R. Liang, Adv. Mater. 35 (2023) e2209692.
[128] Z. Cui, T. Hu, S. Yang, Y. Yang, X. Liu, T. Wang, H. Chen, C. Zeng, R. Liang, Y. Zhou, Chem. Eng. J. 480 (2024).
[129] M. Mo, Y. Jiang, A. Kang, K. Song, H. Qi, J. Li, S. Guan, S. Zhou, ACS Appl. Mater. Interfaces 16 (2024) 23003–23014.
[130] S. Liu, J. Bao, B. Tian, S. Li, M. Yang, D. Yang, X. Lu, X. Liu, S. Gai, P. Yang, Adv. Sci. (Weinh) 11 (2024) e2404146.
[131] L. Wang, Z. Mao, J. Wu, X. Cui, Y. Wang, N. Yang, J. Ge, H. Lei, Z. Han, W. Tang, S. Guan, L. Cheng, Nano Today 49 (2023).
[132] G. Gu, X. Chen, G. Wei, M. Xu, APL Mater. 12 (2024).
[133] Y.-H. Wu, J.-C. Luo, J. Zhang, Z.-C. He, Y. Lan, G.-F. Huang, W. Hu, W.-Q. Huang, Results Phys 54 (2023).
[134] D. Tan, C. Jiang, N. Sun, J. Huang, Z. Zhang, Q. Zhang, J. Bu, S. Bi, Q. Guo, J. Song, Nano Energy 90 (2021).
[135] M. Zhang, D. Yang, C. Dong, H. Huang, G. Feng, Q. Chen, Y. Zheng, H. Tang, Y. Chen, X. Jing, ACS Nano 16 (2022) 9938–9952.
[136] Y. Wu, X. Song, X. Zhou, R. Song, W. Tang, D. Yang, Y. Wang, Z. Lv, W. Zhong, H. L. Cai, A. Zhang, J. Wei, X.S. Wu, Small 19 (2023) e2205053.
[137] X. Zhang, L. Xu, M. Li, X. Chen, J. Tang, P. Zhang, Y. Wang, B. Chen, J. Ren, J. Liu, Materi. Today Nano 24 (2023).
[138] B. Geng, S. Xu, L. Shen, F. Fang, W. Shi, D. Pan, Carbon 179 (2021) 493–504.
[139] G. Li, X. Zhong, X. Wang, F. Gong, H. Lei, Y. Zhou, C. Li, Z. Xiao, G. Ren, L. Zhang, Z. Dong, Z. Liu, L. Cheng, Bioact Mater 8 (2022) 409–419.
[140] J. Xu, X. Wang, Y. Liu, Y. Li, D. Chen, T. Wu, Y. Cao, Acta Biomater. 175 (2024) 307–316.
[141] J. Xu, L. Chen, S. Ding, X. Dai, Y. Dai, Y. Chen, X. Ni, Nano Today 48 (2023).
[142] E. Pang, B. Li, C. Zhou, S. Zhao, Y. Tang, Q. Tan, C. Yao, B. Wang, K. Han, X. Song, Z. Hu, Q. Ouyang, S. Jin, M. Lan, Nanoscale 15 (2023) 16466–16471.
[143] D.Y. Zhang, H. Liu, M.R. Younis, S. Lei, Y. Chen, P. Huang, J. Lin, J. Nanobiotechnol. 20 (2022) 53.
[144] X. Qiao, L. Xue, H. Huang, X. Dai, Y. Chen, H. Ding, J. Nanobiotechnol. 20 (2022) 186.
[145] X. Han, C. Zhao, S. Wang, Z. Pan, Z. Jiang, X. Tang, J. Colloid Interface Sci. 621 (2022) 360–373.
[146] Y. Cao, T. Wu, W. Dai, H. Dong, X. Zhang, Chem. Mater. 31 (2019) 9105–9114.
[147] B. Geng, S. Zhang, X. Yang, W. Shi, P. Li, D. Pan, L. Shen, Chem. Eng. J. 435 (2022).
[148] S. Zhang, L. Zhang, J. Hu, X. He, B. Geng, D. Pan, L. Shen, Chem. Eng. J. 458 (2023).
[149] Y. Zhou, L. Yu, C. Dong, J. Liu, B. Yang, Y. Chen, Z. Hu, Chem. Eng. J. 431 (2022).
[150] Z. Zhou, T. Wang, T. Hu, H. Xu, L. Cui, B. Xue, X. Zhao, X. Pan, S. Yu, H. Li, Y. Qin, J. Zhang, L. Ma, R. Liang, C. Tan, Adv. Mater. 36 (2024) e2311002.
[151] R. Zhao, H. Zhu, L. Feng, Y. Zhu, B. Liu, C. Yu, S. Gai, P. Yang, Small 19 (2023) e2301349.
[152] G. Hu, J. Wang, L. Chen, H. Zheng, Y. Lan, K. Wang, X. Liu, H. You, Y. Luo, L. Dong, Adv. Funct. Mater. 34 (2024).
[153] L. Zhang, T. Yang, L. Ding, M. Chang, X. Yin, Y. Chen, H. Shi, Chem. Eng. J. 484 (2024).
[154] Y. Ding, Y. Zhao, S. Yao, S. Wang, X. Wan, Q. Hu, L. Li, Small 19 (2023) e2300327.
[155] J. Ma, M. Yuan, Z. Yang, Z. Ma, J. Zhang, Z. Li, P. Ma, Z. Cheng, J. Lin, J. Am. Chem. Soc. 146 (2024) 22348–22359.
[156] G. Chen, J. Du, L. Gu, Q. Wang, Q. Qi, X. Li, R. Zhang, H. Yang, Y. Miao, Y. Li, Chem. Eng. J. 482 (2024).
[157] S. Wen, W. Zhang, J. Yang, Z. Zhou, Q. Xiang, H. Dong, ACS Nano 18 (2024) 23672–23683.
[158] Y. Kang, L. Lei, C. Zhu, H. Zhang, L. Mei, X. Ji, Mater. Horiz. 8 (2021) 2273–2285.
[159] Q. Liu, L. Shi, Y. Liao, X. Cao, X. Liu, Y. Yu, Z. Wang, X. Lu, J. Wang, Adv. Sci. (Weinh) 9 (2022) e2200005.
[160] Y. Chen, Z. Tian, X. Wang, N. Ran, C. Wang, A. Cui, H. Lu, M. Zhang, Z. Xue, Y. Mei, P.K. Chu, J. Liu, Z. Hu, Z. Di, Adv. Mater. 34 (2022) e2201630.
[161] S. Chae, S.S. Chae, M. Choi, H.M. Park, H. Chang, J.-O. Lee, T. Il Lee, Nano Energy 56 (2019) 65–73.
[162] A.L. Friedman, A.T. Hanbicki, F.K. Perkins, G.G. Jernigan, J.C. Culbertson, P. M. Campbell, Sci. Rep. 7 (2017) 3836.
[163] X. Ma, B. Ding, Z. Yang, S. Liu, Z. Liu, Q. Meng, H. Chen, J. Li, Z. Li, P. Ma, J. Lin, J. Am. Chem. Soc. 146 (2024) 21496–21508.
[164] M.M. Alyörük, Y. Aierken, D. Çakır, F.M. Peeters, C. Sevik, J. Phys. Chem. C 119 (2015) 23231–23237.
[165] Y. Yang, J. Ge, G. Li, H. Lei, L. Chen, Y. Gong, X. Zhong, L. Wang, Y. Dai, W. Tang, J. Zou, Y. Cheng, Z. Liu, L. Cheng, Nano Today 46 (2022).
[166] Q. Truong Hoang, K.A. Huynh, T.G. Nguyen Cao, J.H. Kang, X.N. Dang, V. Ravichandran, H.C. Kang, M. Lee, J.E. Kim, Y.T. Ko, T.I. Lee, M.S. Shim, Adv. Mater. 35 (2023) e2300437.
[167] H. Lei, X. Wang, S. Bai, F. Gong, N. Yang, Y. Gong, L. Hou, M. Cao, Z. Liu, L. Cheng, ACS Appl. Mater. Interfaces 12 (2020) 52370–52382.
[168] Y. Zhu, K. Shen, Y. Wang, Q. Yang, X. Li, A. Pan, Z. Xie, H. Yin, Q. Tian, F. Zhang, G. Fang, Ind. Crop. Prod. 215 (2024).
[169] M. Wu, J. Yong, H. Zhang, Z. Wang, Z.P. Xu, R. Zhang, Adv. Healthc. Mater. 12 (2023) e2301497.
[170] Y. Zhao, T. Huang, S. Wang, S. Yao, Q. Hu, X. Wan, N. Guo, Y. Zhang, L. Li, J. Colloid Interface Sci. 640 (2023) 839–850.

[171] Y. Kang, Z. Mao, Y. Wang, C. Pan, M. Ou, H. Zhang, W. Zeng, X. Ji, Nat. Commun. 13 (2022) 2425.
[172] X. Li, B. Zhou, M. Fan, C. Xia, F. Xu, Q. He, Nano Energy 131 (2024).
[173] J. Xu, Y. Liu, H. Wang, J. Hao, Y. Cao, Z. Liu, Acta Biomater. 188 (2024) 344–357.
[174] W. Chen, C. Liu, X. Ji, J. Joseph, Z. Tang, J. Ouyang, Y. Xiao, N. Kong, N. Joshi, O. C. Farokhzad, W. Tao, T. Xie, Angew. Chem. Int. Ed. Eng. 60 (2021) 7155–7164.
[175] S. Lin, M. Yang, J. Chen, W. Feng, Y. Chen, Y. Zhu, Small 19 (2023) e2204992.
[176] L. Cai, J. Du, F. Han, T. Shi, H. Zhang, Y. Lu, S. Long, W. Sun, J. Fan, X. Peng, ACS Nano 17 (2023) 7901–7910.
[177] S. Mula, L. Dona, B. Civalleri, M.A. van der Veen, ACS Appl. Mater. Interfaces 14 (2022) 50803–50814.
[178] C. Zhang, D. Lei, C. Xie, X. Hang, C. He, H.L. Jiang, Adv. Mater. 33 (2021) e2106308.
[179] T. Hu, T. Wang, Y. Yang, C. Yu, J. Yu, R. Liang, W. Ji, Chem. Eng. J. 505 (2025).
[180] Q. Wang, Y. Tian, M. Yao, J. Fu, L. Wang, Y. Zhu, Adv. Mater. 35 (2023) e2301784.
[181] X. Zhong, X. Li, L. Gu, H. Yang, J. Du, Q. Wang, Y. Li, Y. Miao, J. Colloid Interface Sci. 679 (2025) 354–363.
[182] L. Hang, M. Li, Y. Zhang, W. Li, L. Fang, Y. Chen, C. Zhou, H. Qu, L. Shao, G. Jiang, Small 20 (2024) e2306364.
[183] G. Lin, G.T. Nash, T. Luo, I. Ghosh, S. Sohoni, A.J. Christofferson, G. Liu, G. S. Engel, W. Lin, Adv. Mater. 35 (2023) e2212069.
[184] Z. Zhou, T. Wang, T. Hu, C. Cheng, S. Yu, H. Li, S. Liu, L. Ma, M. Zhao, R. Liang, C. Tan, Mater. Chem. Front. 7 (2023) 1684–1693.
[185] S. Jiang, C. Liu, Q. He, K. Dang, W. Zhang, Y. Tian, Nano Res 16 (2023) 9633–9641.
[186] Y. Duan, Y. Yu, P. Liu, Y. Gao, X. Dai, L. Zhang, L. Chen, Y. Chen, Angew. Chem. Int. Ed. Eng. 62 (2023) e202302146.
[187] R. Wu, M. Hua, Y. Lu, L. Chen, Y. Chen, Z. Hu, Angew. Chem. Int. Ed. Eng. 64 (2025) e202416461.
[188] X. Xiao, Y. Zhao, P.A. Ma, Z. Cheng, J. Lin, Chem. Eng. J. 440 (2022).
[189] L. Yang, B. Tian, Y. Xie, S. Dong, M. Yang, S. Gai, J. Lin, Adv. Mater. 35 (2023) e2300648.
[190] W. Zhang, M. Fan, R. Yang, Z. Li, Y. Qiu, M. Dong, P. Song, N. Wang, Y. Yang, Q. Wang, J. Mater. Chem. B 12 (2024) 7892–7904.
[191] C. Dai, S. Zhang, Z. Liu, R. Wu, Y. Chen, ACS Nano 11 (2017) 9467–9480.
[192] F. Wang, B. Wang, W. You, G. Chen, Y.Z. You, Nano Res 15 (2022) 9223–9233.
[193] Z. Lv, L. Jin, Y. Cao, H. Zhang, D. Xue, N. Yin, T. Zhang, Y. Wang, J. Liu, X. Liu, H. Zhang, Light Sci Appl 11 (2022) 116.
[194] L. Wang, M. Niu, C. Zheng, H. Zhao, X. Niu, L. Li, Y. Hu, Y. Zhang, J. Shi, Z. Zhang, Adv. Healthc. Mater. 7 (2018) e1800819.
[195] R.L. Perlman, Evol. Med. Public Health 2016 (2016) 170–176.
[196] Y.H. Bae, K. Park, J. Control. Release 153 (2011) 198–205.

Nam Anh Tran received B.Eng (Hons) and M.Sc (HD) degrees in Chemical Engineering and Biochemistry from Ho Chi Minh City University of Technology (HCMUT) and Soongsil University (Seoul, Korea), in 2016 and 2019, respectively. From 2019 to 2020, he worked as researcher at Biophysical Chemistry Lab (Soongsil University). Currently, he is PhD Student at Griffith University. His research focuses on 2D materials, metal oxides nanoparticles and their applications in catalysis, gas barrier and cancer therapies.

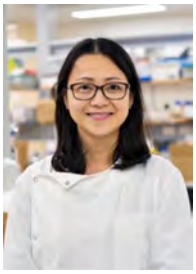

Hang Thu Ta is a professor of materials science at the School of Environment and Science, and Queensland Quantum and Advanced Technologies Research Institute, Griffith University, Australia. She is an ARC Future Fellow, Heart Foundation Future Leader Fellow, and has a unique skill set combining chemistry and biology. She got a PhD from University of Melbourne in 2009 and then worked at the Baker Heart and Diabetes Institute and University of Queensland before moving to Griffith University in 2020. Her research is focused on 1) bio/nanomaterials for diagnosis and treatment of life-threatening diseases, 2) organs-on-a-chip, 3) surface coating materials, and 4) cell delivery and therapy.